Environmental Science and Pollution Research (2022) 29:69294–69326
https://doi.org/10.1007/s11356-022-22550-7

REVIEW ARTICLE

Nanomaterials photocatalytic activities for waste water treatment: a review

Permender Singh[1] · Brij Mohan[2] · Vasundhara Madaan[1] · Rohit Ranga[1] · Parveen Kumari[1] · Sandeep Kumar[3] · Vinita Bhankar[4] · Parmod Kumar[5] · Krishan Kumar[1]

Received: 3 June 2022 / Accepted: 11 August 2022 / Published online: 17 August 2022

Abstract

Water is necessary for the survival of life on Earth. A wide range of pollutants has contaminated water resources in the last few decades. The presence of contaminants incredibly different dyes in waste, potable, and surface water is hazardous to environmental and human health. Different types of dyes are the principal contaminants in water that need sudden attention because of their widespread domestic and industrial use. The toxic effects of these dyes and their ability to resist traditional water treatment procedures have inspired the researcher to develop an eco-friendly method that could effectively and efficiently degrade these toxic contaminants. Here, in this review, we explored the effective and economical methods of metal-based nanomaterials photocatalytic degradation for successfully removing dyes from wastewater. This study provides a tool for protecting the environment and human health. In addition, the insights into the transformation of solar energy for photocatalytic reduction of toxic metal ions and photocatalytic degradation of dyes contaminated wastewater will open a gate for water treatment research. The mechanism of photocatalytic degradation and the parameters that affect the photocatalytic activities of various photocatalysts have also been reported.

Keywords Photocatalytic degradation · TiO_2 · Organic waste · Wastewater treatment · Dye decomposition

Introduction

Water pollution is a critical global issue that has recently received much attention due to its severe adverse impacts on life and the environment of the planet. Because water is essential for developing and sustaining a healthy life, finding clean and fresh potable water is likely the biggest difficulty that modern society is facing (Baron 2008; Karim et al. 2022). The water resources are exploited due to domestic, industrial, agricultural, and municipal activities. It is because of these activities, a significant amount of harmful contaminants such as heavy metal ions (Zn, Cu, Pb, Ni, Cd, Hg, etc.), organic dyes, toxic gases, herbicides, pesticides, hydrocarbons, and pharmaceuticals enter ground- and freshwater bodies (Reemtsma et al. 2006; Boroski et al. 2009). Even a small amount of these toxic substances could result in serious health problems because these substances are carcinogens and cause genetic mutations.

Consequently, these substances negatively impact neural systems and significantly harm a variety of organs, including the respiratory system, reproductive system, and gastrointestinal tract (Carolin et al. 2017; Mojiri et al. 2019;

Responsible Editor: Sami Rtimi

Permender Singh and Brij Mohan contributed equally to the manuscript.

✉ Krishan Kumar
krishankumar.chem@dcrustm.org

[1] Department of Chemistry, Deenbandhu Chhotu Ram University of Science & Technology, Murthal, Sonepat 131039, Haryana, India

[2] College of Ocean Food and Biological Engineering, Jimei University, 185 Yinjiang Road, Jimei District, Xiamen 361021, China

[3] Department of Chemistry, J. C. Bose University of Science & Technology, YMCA, Faridabad 126006, Haryana, India

[4] Department of Biochemistry, Kurukshetra University, Kurukshetra 136119, Haryana, India

[5] Department of Physics, J. C. Bose University of Science & Technology, YMCA, Faridabad 126006, Haryana, India

Hassani et al. 2020a, b; Zhang et al. 2020; Trellu et al. 2021). As a result, contamination of freshwater reservoirs by toxic materials directly or indirectly has significantly resulted in the loss of water quality and the lack of freshwater resources. Therefore, there is a rapidly expanding need for proper, sustainable water management strategies and more advanced water treatment technologies. Several conventional techniques for upgrading water quality by reducing toxic heavy metal ions to their fewer toxic or non-toxic forms and degradation of different organic dyes in wastewater have been implemented. These techniques include adsorption (Alidokht et al. 2013; Sirajudheen et al. 2020), biological treatment (Rana et al. 2018; Fang et al. 2020), desalination (Luo et al. 2012; Khairkar et al. 2020), electrocoagulation (Ghanbari et al. 2020; Nidheesh et al. 2021), flocculation (Teh et al. 2016; Tang et al. 2020), ion exchange (Bolto et al. 2002; Nabi et al. 2010), membrane separation (Nataraj et al. 2006; Castro-Muñoz et al. 2021), and reverse osmosis (Mondal et al. 2013; Albergamo et al. 2020). However, these methods have many drawbacks (Ibrahim et al. 2016), including the excessive amount of sludge formation, consumption of high energy, low removal efficiency & expensive and generation of secondary pollutants (Selvasembian and Balasubramanian 2018; Gunarathne et al. 2020; Singh et al. 2020; Shabaan et al. 2020). Therefore, developing a reliable and effective method to treat various pollutants has become necessary.

As a result, the focus needs to be done on improving/innovating environmentally friendly, low-energy, and cost-effective technologies for water purification. To address these issues, developing an innovative, environmentally friendly, and economical technology that can remove wastewater contaminants with minimum energy consumption and chemical usage is critical. Consequently, researchers have concentrated on advanced oxidation processes (AOPs) as robust alternative procedures that are competent to oxidize and mineralize a wide spectrum of organic chemicals because of their strongly oxidizing and highly potent radicals. AOP is an aqueous phase oxidation technique that uses in situ production of powerful oxidizing agents, including hydroxyl radicals ($^{\bullet}OH$) and sulfate radicals ($SO_4^{\bullet -}$) to speed up the oxidation of contaminants found in water and wastewater (Ghanbari and Moradi 2017; Miklos et al. 2018; Babu et al. 2019). Due to their effectiveness and efficiency in completely mineralizing or converting various pollutants into less hazardous substitutes from wastewater, AOPs have gathered much attention (Oturan and Aaron 2014; Rana et al. 2018; Eghbali et al. 2019). Fast degradation rates and non-selectivity in the oxidation of pollutants are additional benefits of AOPs. To remove water contaminants, AOPs use a variety of processes, such as moist air oxidation, Fenton's process, ozonation, photocatalysis, sonolysis, and sulfate radicals-based AOPs (SR-AOPs) (Nidheesh et al. 2013; Ghanbari and Moradi 2017; Surenjan et al. 2019; Brillas 2020; Malik et al. 2020; Ghanbari et al. 2021; Pourshirband and Nezamzadeh-Ejhieh 2021; Wang et al. 2021; Zhang and Chu 2022).

Chemical agents such as metals, O_3, or H_2O_2 and an assisting energy source including ultraviolet or visible light, ultrasound, current, or γ-irradiation are frequently used in AOPs (Braun 2003). For instance, AOPs include (Giannakis et al. 2017):

(i) Fenton-related terms, such as photo-Fenton and electro-Fenton (Fe/H_2O_2).
(ii) γ-radiolysis
(iii) Heterogeneous photocatalysis, including that involving (TiO_2/hv)
(iv) Based on ozone: O_3/H_2O_2, O_3/UV, and O_3/UV/H_2O_2
(v) Ultrasound-based: sonolysis, Fenton assisted by ultrasound
(vi) Based on UV: UV, UV/H_2O

Photocatalysis, in addition to AOP, has been proven to be an effective way to improve the biodegradability of persistent organic pollutants while also removing present and emerging microbial pathogens. Photocatalytic oxidation is a group of reactions that utilize a catalyst triggered by chemical, solar, or other forms of energy and rely on the formation of strong reactive radical species like $O_2^{\bullet -}$, O_3, H_2O_2, and mostly $^{\bullet}OH$ radical. These radicals are strongly oxidizing in nature and degrade all organic molecules present in water non-selectively (Huang et al. 2000; Kudo et al. 2003; Pera-Titus et al. 2004; Bahnemann 2004; Wang and Xu 2012; Ottman et al. 2019). In recent years, light-absorbing catalysts (photocatalysts) have found promising applications in degrading toxic dyes and reducing heavy metal ions to their lesser toxic forms. Photocatalysts have higher catalytic efficiencies, take a small interval for the reactions, and do not form secondary hazardous products (Ramya et al. 2022). Recent studies have acknowledged photocatalytic hydrogen production as an effective substitute for global energy resources. Photocatalysis is triggered by photons of light obtained from solar energy under ideal conditions despite the lack of thermal energy. Many semiconductors are being utilized in photocatalysis that produces strongly energetic holes (h^+) and electrons (e^-) when exposed to UV light. Electron–hole couples may create reactive oxygen species (ROS) particularly $^{\bullet}OH$ and $O_2^{\bullet -}$ radicals with highly oxidizing properties that can migrate to the outer section and trigger oxidation and reduction reactions. Solar energy is converted into chemical energy and other chemical by-products by reducing H_2O, which generated hydrogen and other hydrocarbons (Li et al. 2010; Sakimoto et al. 2016).

Recent studies have shown that the photocatalysts can be magnetized by making composites with materials such

as Ag_xO, Cu_xO, or FeO_x. Such doping of photocatalysts with Ag_xO, Cu_xO, or FeO_x increases the solar light absorption (Cattarin and Decker 2009). The other advantage of such photocatalysts composite is the low cost of separation. However, there are also some disadvantages of these magnetic photocatalysts including the lack of experimental data and information to analyze, characterize, and explain the interaction between light waves and magnetic materials. In the accessible scientific literature, there is either little or no information available about the toxicity and cytotoxicity of magnetic photocatalysts (Kiwi and Rtimi 2021) (Table 1).

This review article emphasizes the importance of various photocatalysts, including doped, green synthesized and magnetic photocatalysts for the removal of different organic pollutants (dyes) and degradation of various toxic heavy metal ions from aquatic environments. The basic principle behind the photocatalytic degradation of organic dyes and the factors affecting photocatalytic degradation has been explained. The advantages of using nanosized photocatalysts over traditional photocatalysts have also been explored. Several techniques used for the synthesis of these photocatalysts are also examined. Furthermore, the potential future advancements and related perspectives are explained.

Methods of preparation of photocatalysts

Sol–gel method

One of the popular liquid phase techniques for fabricating homogenous metal oxide photocatalysts is the sol–gel approach. This technique has been widely employed since the resulting product has a high porosity level, a vast surface area, and the capacity to maintain thermal equilibrium. The shortcomings of conventional procedures, such as the heterogeneities of the final product, the high temperature

Table 1 Comparative table with selectivities of different catalysts

Sr. no	Photocatalyst	Method of synthesis	Morphology	Light source	Dye degraded	Efficiency	Reference
1	$Ag_xO/FeO_x/ZnO$	Photochemical reduction	Nanotubes	Suntest solar simulator	Tetracycline	85% (within 240 min)	(Yu et al. 2019b)
2	TiO_2/FeO_x/POM	Hydrothermal method	Nanopores and micropores	Low-intensity solar light	2,4-dichlorophenol	55.9%	(Yu et al. 2019c)
3	Fe@MWCNT		Semi-spherical	UVA-LED w	Azorubine	95%	(Madihi-Bidgoli et al. 2021)
4	($CoFe_2O_4$/mpg-C_3N_4 (Sonocatalyst)	Thermal decomposition and liquid phase self-assembly method	Nanosheets	Ultrasonic bath apparatus (WUC-D10H, 40 kHz, 665 W	Methylene blue (MB)	92.81%	(Hassani et al. 2018)
5	$CoFe_2O_4$/mpg-C_3N_4	Liquid self-assembly technique	Nanosheets		Acetaminophen	> 92%	(Hassani et al. 2020a)
6	Z-scheme CdS/g-C_3N_4		Semi-spherical (CdS) and nano sheet (g-C_3N_4)	100 W tungsten lamp for 90 min	Methyl orange (MO)	> 85%	(Pourshirband and Nezamzadeh-Ejhieh 2021)
7	Cu–TiO_2/Zn–TiO_2	Sol–gel method and simple physical mixing	Spherical	UVA-LED	Bisphenol S	100% in 18 min	(Zhang and Chu 2022)
8	Polyethylene-TiO_2			Low-intensity solar simulated light	MB	98%	(Rtimi et al. 2015)
9	TiO_2 impregnated polyester	Ultrasonication		UV and visible light	Reactive Green 12 (RG12)	100% under UV light and 87.14% under visible light within 120 min	(Zeghioud et al. 2017)
10	Cu_xO/TiO_2	High-power impulse magnetron sputtering		Visible light light-emitting diodes	RG12	53.4%	(Zeghioud et al. 2019)
11	Hybrid acrylic/TiO_2 films	miniemulsion polymerization	A continuous TiO_2 NPs network	Low-intensity simulated sunlight	*Escherichia coli* (bacterial inactivation)	100% within 240 min	(Bonnefond et al. 2015)

(1100–1300 °C) needed for the reaction, and the possibility of air pollution from the discharge of ash particles, can also be overcome by utilizing this type of synthesis technique. The sol–gel technique can be classified into two categories based on the reaction process. An aqueous/hydrolytic sol–gel method is the one when water is used as the reaction medium; a non-aqueous sol–gel method involves an organic solvent (such as alcohol, ketone, or ether) as the reaction medium. These days, acids and bases are utilized to hydrolyze metal alkoxide, in addition to water and alcohol (sol–gel). Because they are very easy to purify and have excellent solubility, the metal alkoxides from the precursor are regarded as the best.

Five processes are involved in the procedure: hydrolysis, condensation, aging, drying, and calcination. It can be summed up as follows: the precursor is broken down during hydrolysis, and a suitable solvent is employed. Afterwards condensation in this process, a metal oxide bond is created by removing the water and alcohol. In the end, this process increases the solvent's viscosity while retaining the liquid phase gel. The viscous complex expands rapidly during the third stage of aging because a solvent is trapped down between the gel. Sol particles aggregate due to ongoing condensation and precipitation in the process. One of the crucial and challenging steps in the drying process is the solvent removal from the gel, which significantly impacts the final product. To get the required product, many drying procedures might be used. Correspondingly, aerogel, xerogel, and cryogen are produced *via* superficial thermal and freeze-drying methods. The final task includes calcination, which improves the mechanical characteristics by removing the remaining water molecule from the final sample (Yadav et al. 2022).

Multi-doped NSC-TiO_2 was fabricated by Lei et al. using the sol–gel method in association with a high-energy ball milling technique (Lei et al. 2015). The harmful Cr(VI) metal ion may be reduced to the less hazardous Cr(III) ion using the multi-doped NSC-TiO_2. Ahmad et al. used a sol–gel approach (Fig. 1) to fabricate a nanostructured ZnO/$SrZnO_2$ composite that functions as a powerful visible light-triggered photocatalyst (Ahmad et al. 2022). Under visible light irradiation, the developed photocatalyst mineralized the azo dye (Congo red, CR) and eliminated the bacterial strain (*Escherichia coli*, *E-coli*). According to the results of the photocatalytic tests, the ZnO/$SrZnO_2$ composite had a greater photocatalytic efficiency, mineralizing 92.4% of the CR dye in comparison to $SrZnO_2$ (57.9%) and ZnO (34.6%) (Ahmad et al. 2022).

Electrochemical anodization method

Another method for fabricating metal oxide nanotube photocatalysts, such as TiO_2, is electrochemical anodization. The surface porosity and morphology of the photocatalyst can be improved by electrochemical anodization at room temperature (Lin et al. 2013; Ayati et al. 2016; Robinson Aguirre and Félix Echeverría 2018). In this technique, thin metal sheets were employed as the cathode (working electrode) and other sheets, such as graphite, as the anode (counter electrode). Then, electrochemical anodization is performed

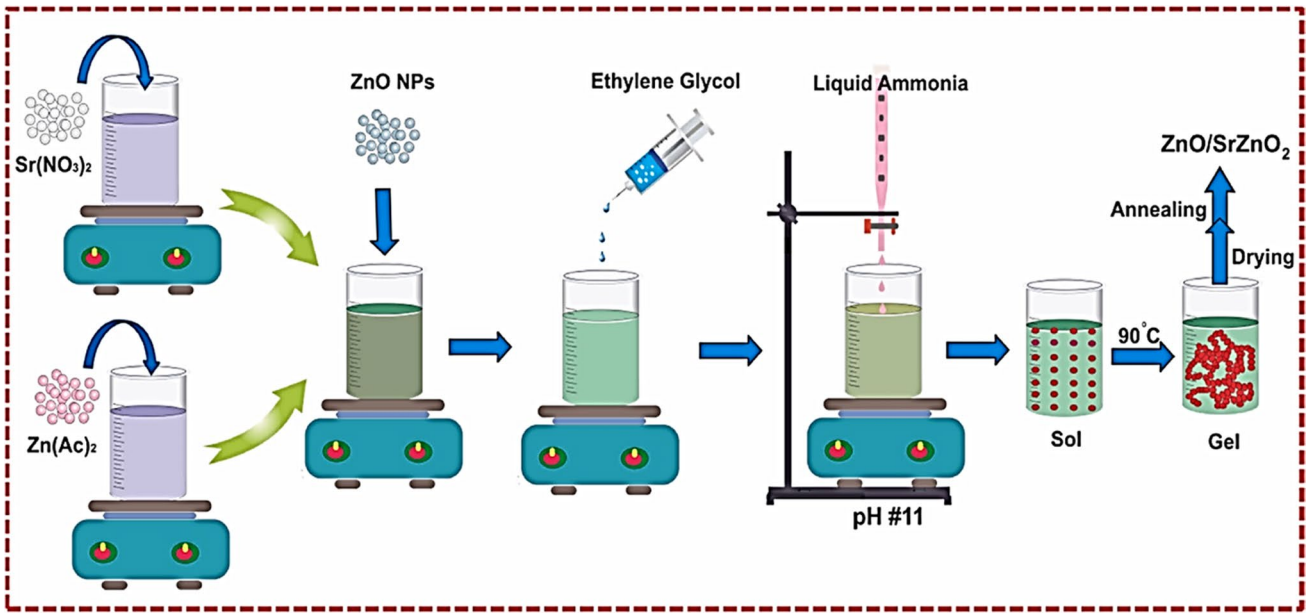

Fig. 1 Schematic represenrataion of fabrication of ZnO/$SrZnO_2$ nanocomposite *via* a sol–gel route. Reproduced with permission, copyright © 2020 Elsevier Ltd, (licence number — 5,362,460,622,777). All rights reserved. (Ahmad et al. 2022)

for a specific time using a suitable solvent and electrolyte and maintaining a specified distance between the electrodes. The anodization voltage can be varied. This technique is simple and cost-effective (Khaw et al. 2019). In contrast to the powder form, metal oxide nanotube sheets are also easy to separate and recover. Rojviroon et al. synthesized TiO_2 nanotubes photocatalyst *via* electrochemical anodization (Fig. 2) and reported the photocatalytic decolourization of Reactive Black 5 (RB5) and indigo carmine (IC) dyes using fabricated TiO_2 nanotubes (Rojviroon et al. 2021).

Hydrothermal/solvothermal method

The hydrothermal/solvothermal method involves a chemical reaction in aqueous or non-aqueous solvents like CH_3OH or C_2H_5OH in sealed vessels where the temperature of the solvents can be raised to close to their critical points by heating and to apply autogenous pressures at the same time. This process is known as hydrothermal when water is employed as the solvent. It is referred to as solvothermal when methanol or ethanol is utilized as the solvent. The best approach for synthesizing single crystals and nanomaterials photocatalysts is the hydrothermal method, in which the solubility of reactant precursors depends on hot water under high pressure. Using a hydrothermally synthesized TiO_2 that had been modified to form a magnetically separable TiO_2/FeO_x microstructure decorated with poly-oxo-tungstate (POM), Yu et al. demonstrated the photocatalytic degradation of 2,4-dichlorophenol (2,4-DCP) (Yu et al. 2019c). Chen et al. described the synthesis of zinc sulfide (ZnS) microspheres photocatalyst *via* the hydrothermal method (Chen et al. 2016b). The photocatalytic activity of as-synthesized samples was assessed by evaluating the degradation efficiency of MB in the presence of photocatalysts. More than 60% of the original dye was degraded after 3 h of radiation. Using a hydrothermal process, Baeissa et al. reported the fabrication of sodium niobate ($NaNbO_3$) (Baeissa 2016). Then doping of sodium niobate nanocubes with gold was done. The resulting $NaNbO_3$ doped with gold ($Au/NaNbO_3$) found potential application for the degradation of malachite green (MG) dye. Shammi et al. reported the fabrication of $CuO\text{-}VO_2/TiO_2$ as a new nanocomposite via a hydrothermal route. The as-synthesized $CuO\text{-}VO_2/TiO_2$ nanocomposite demonstrated photocatalytic degradation of methylene blue (MB), methyl orange (MO), and Congo red (CR) under visible irradiations (Shammi et al. 2021). The hydrothermal approach was used by Madona and Sridevi to fabricate a $MgO/g\text{-}C_3N_4$ heterojunction nanocomposite as shown in Fig. 3 (Madona and Sridevi 2022). In comparison to pure MgO and $g\text{-}C_3N_4$, the produced $MgO/g\text{-}C_3N_4$ nanocomposite demonstrated high photocatalytic performance through the degradation of MG when exposed to solar light. After five trials, the $MgO/g\text{-}C_3N_4$ nanocomposite exhibits good stability and high degrading efficiency. MG dye removal by the MgO/g-C3N4 catalyst achieved the greatest rate constant of 0.1079 min^{-1}, which is about 5.3 and 13.6 times superior to MgO (0.0207 min^{-1}) and $g\text{-}C_3N_4$ (0.00789 min^{-1}), correspondingly (Madona and Sridevi 2022). Furthermore, the antibacterial efficacy of the $MgO/g\text{-}C_3N_4$ nanocomposite against Gram-positive and Gram-negative bacteria like *S. aureus*, *B. subtilis*, and *E. coli*, *P. aeruginosa*, was examined. Due to the generation of reactive oxygen species, the zone

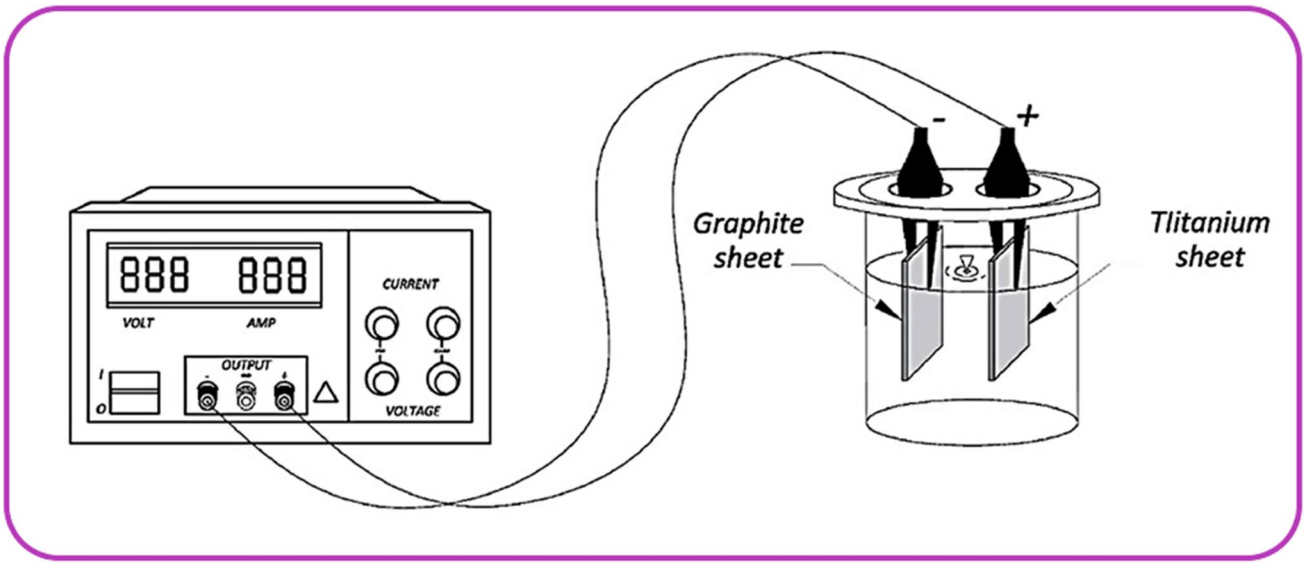

Fig. 2 Schematic representation of electrochemical anodization method for the fabrication of TiO_2 nanotube. Reproduced with permission, copyright © 2020 Elsevier Ltd, (licence number — 5,362,431,451,027). All rights reserved (Rojviroon et al. 2021)

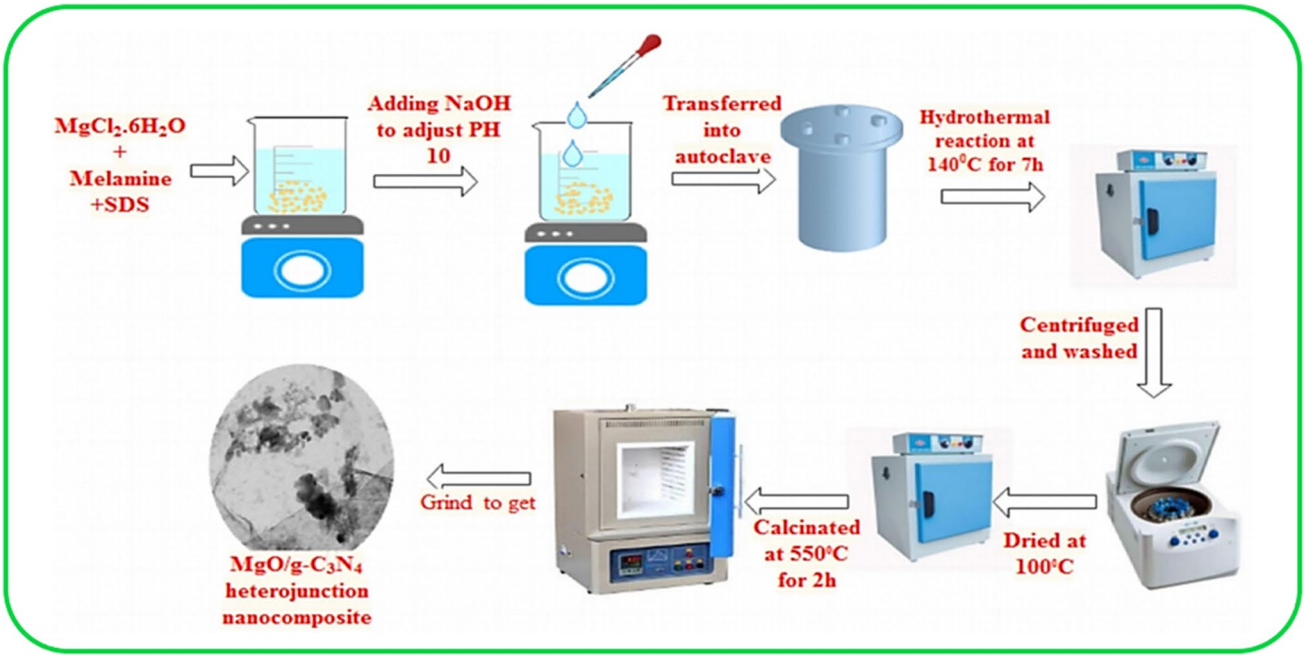

Fig. 3 Representation of a hydrothermal route for the synthesis of MgO/ g-C_3N_4 heterojunction nanocomposite. Reproduced with permission, copyright © 2020 Elsevier Ltd, (licence number 5362500354972). All rights reserved (Madona and Sridevi 2022)

of inhibition is seen in the range of 6 to 7 mm and grows with increasing MgO/g-C_3N_4 nanocomposite concentration (ROS).

Co-precipitation method

Potentially toxic ions and dyes can be removed from water by using the metal oxides photocatalysts produced by co-precipitation. The co-precipitation technique is reliable for synthesizing magnetic nanoparticles photocatalysts of nano-ferrite, cobalt oxide, and zinc sulfide. This approach can be used to produce the material in bulk. In addition, it is a quick and adaptable method of purification that can be used to remediate contaminated industrial sewage. Moreover, this technique is particularly effective in removing pollutants from wastewater in ppm amounts. Mani et al. reported the green fabrication of zinc sulfide (ZnS) nanoparticles (NPs) *via* a simple co-precipitation method from plant extracts (Mani et al. 2018). The ZnS was demonstrated to cause photocatalytic degradation of MB dye and MO dye. Thilagavathi et al. used a facial co-precipitation approach to fabricate WO_3/$CoWO_4$ nanocomposite (Fig. 4) which have potential to degrade toxic MB dye in the presence of UV-A light (Thilagavathi et al. 2021). Seventy percent of the natural color of MB was eliminated using pure WO_3. However, the photocatalytic decolorization of MB was improved when cobalt was added into the WO_3 lattice: the sample with 5 wt% Co catalyzed the decolorization of MB by 74.7%, while the sample with 20 wt% Co catalyzed the decolorization of Mb by 86.5% (Thilagavathi et al. 2021).

Sonochemical method

The study of the consequences of phenomenal reactions and the use of ultrasonic waves is known as sonochemistry. The sonochemical process involves irradiating an aqueous medium with ultrasound (20 kHz–10 MHz), which operates on the theory of acoustic cavitations. In the medium, bubbles can be created, enlarged, and collapsed. This generates a pressure of 500 atm and a temperature of about 5000 °C. This approach is applicable to chemical processes that take place in both liquid–solid and homogeneous liquid systems. By using a straightforward sonochemical process, Ayodhya et al. reported the green production of capped cadmium sulfide (CdS) nanoparticles (NPs) from *C. gigantea* leaf extract as shown in Fig. 5 (Ayodhya and Veerabhadram 2017). In addition, these CdS NPs were reported to show the photocatalytic degradation of MB and eosin yellow (EY) dyes.

Ultra-sonication

Chauhan et al. reported the preparation of ZnO nanoflowers/graphene oxide (ZnO/GO) composite over Si substrate in order to degrade MB dye in the presence of solar light (Chauhan et al. 2019). In the first step, zinc acetate dihydrate and isopropyl alcohol were ultrasonically processed

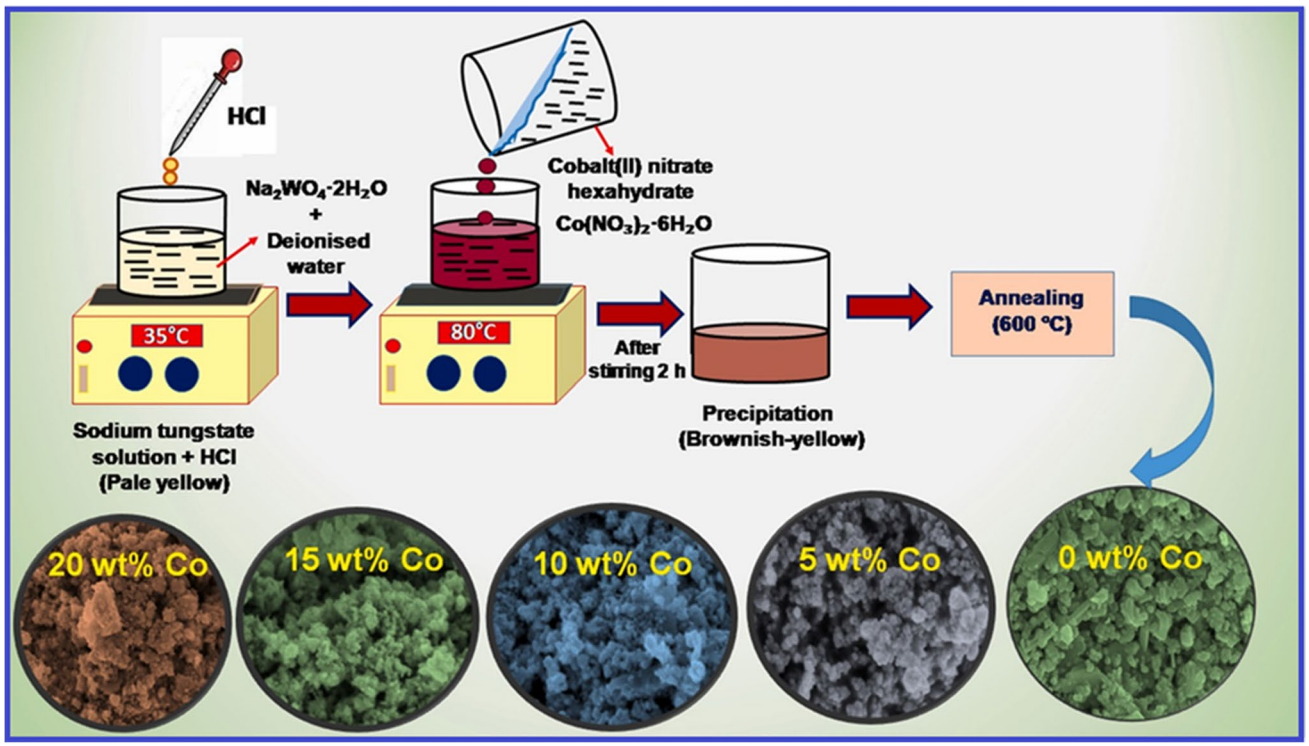

Fig. 4 Schematic representation of a facial co-precipitation method for the fabrication of pure WO_3 nanoparticles and WO_3/$CoWO_4$ nanocomposites. Reproduced with permission, copyright © 2020 Elsevier Ltd, (licence number 5362481064137). All rights reserved (Thilagavathi et al. 2021)

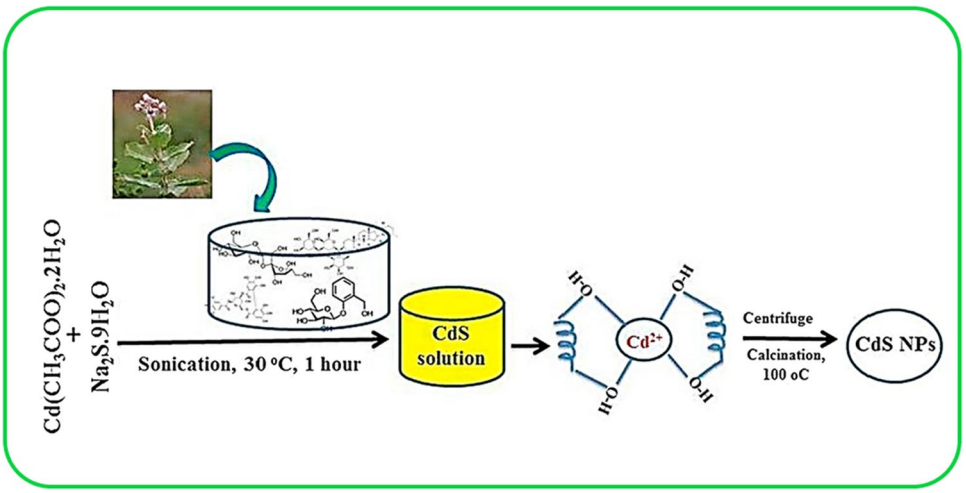

Fig. 5 The schematic diagram of *C. gigantea* leaf extract capped CdS NPs under sonochemical method. Reproduced with permission, copyright © 2020 Elsevier Ltd, (licence number — 5,362,451,112,570). All rights reserved (Ayodhya and Veerabhadram 2017).

to obtain ZnO nanoseeds. To create a ZnO/GO nanocomposite, these ZnO nanoseeds are mixed with graphene oxide (GO). Figure 6 illustrates the various processes involved in the fabrication process.

Magnetron sputtering of thin films

For the inactivation of bacteria, Rtimi and his colleagues reported the fabrication of adhesive, uniform TiO_2 layer

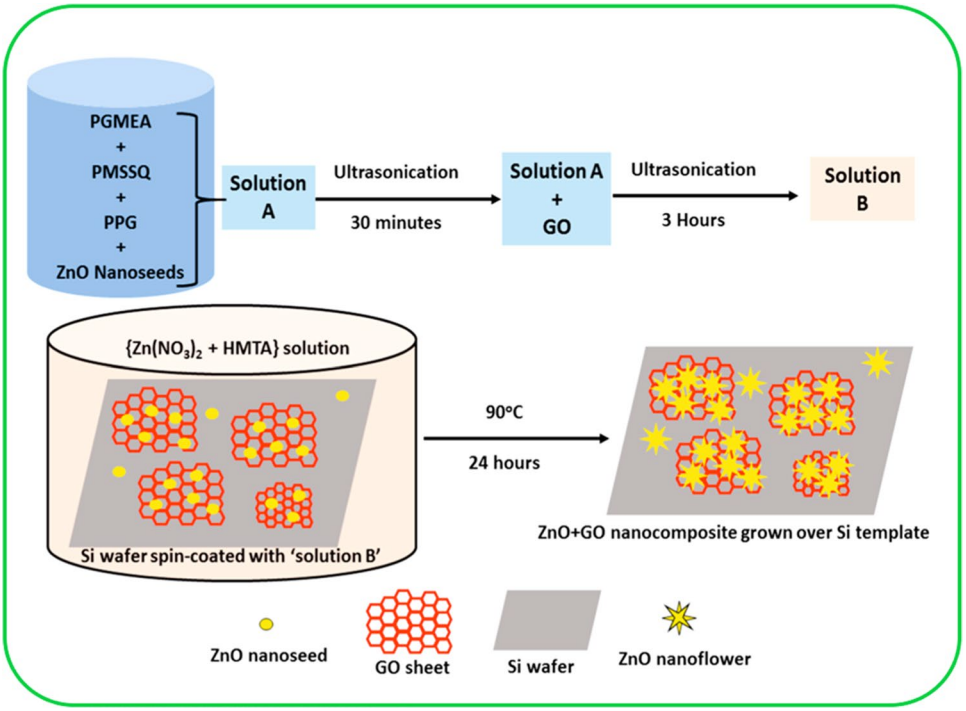

Fig. 6 The schematic illustration of the fabrication procedures for producing a ZnO/GO nanocomposite. Reproduced with permission, copyright © 2020 Elsevier Ltd, (licence number — 5,347,500,540,999). All rights reserved (Chauhan et al. 2019). PGMEA, propylene glycol methyl ether acetate, PMSSQ, polymethylsilsesquioxane, PPG, polypropylene glycol

photocatalysts using direct current magnetron sputtering (DCMS) and high power impulse magnetron sputtering (HIPIMS) (Rtimi et al. 2016). In the presence of visible light-emitting diodes (LEDs) illumination, Zeghioud and his colleagues demonstrated the degradation of RG12 dye by Cu_xO/TiO_2 photocatalyst produced using high-power impulse magnetron sputtering (HiPIMS) (Zeghioud et al. 2019). Grao et al. used pulsed DC magnetron sputtering to deposit crystalline TiO_2 on stainless-steel mesh in a single step without the use of annealing, substrate heating, substrate bias, or extra energy supplies (Grao et al. 2020). Under UV-A, this TiO_2-coated stainless-steel mesh efficiently degraded the three most popular dyes employed in photocatalysis: MB, MO, and RhB. Furthermore, after 10 consecutive cycles, there was little or no loss of photocatalytic activity (Grao et al. 2020).

Using Cu_2O photocatalyst target material, Görgün et al. reported the fabrication of nanofibers made of polyvinylidene fluoride-co-hexafluoropropylene (PVDF-HFP) using an electrospinning approach on an aluminum substrate. Under a 105 W tungsten light bulb, it was discovered that the photocatalysts could decolorize MB with a maximum yield of 76% (Görgün et al. 2019). Meng et al. described the photocatalytic activity of TiO_2 thin films deposited by radio-frequency (RF) magnetron sputtering. RF magnetron sputtering with a ceramic TiO_2 target was used to create nano-TiO_2 thin films on silicon and glass substrates (Meng et al. 2009). Using a high-pressure mercury lamp as a lamp-house, the photocatalytic activity was assessed by measuring the light-induced degradation of a 5-ppm MO solution. The film was employed six times in the degradation of 5 ppm MO, with the rates of degradation being 36.566%, 33.112%, 32.824%, 32.248%, 30.521%, and 28.794%, respectively.

Basic principle of photocatalytic degradation of organic dyes

The main principle behind photocatalytic degradation involves a semiconductor comprising a valence band (VB) and conduction band (CB) in its electronic structure (Amanulla et al. 2022). These bands have an energy gap between them called a bandgap (Hosseini-Zori 2018). When illuminated by photons having energy ≥ bandgap energy, the electron present in the valence band is excited to the CB, generating a positively charged hole in the VB. Both hole and electron are strongly oxidizing and reducing species, respectively. When the hole and electron react with H_2O molecules, hydroxyl (•OH) and superoxide (O_2•−) radicals are generated, which attack the organic dyes and convert them into non-hazardous compounds like CO_2 and H_2O (Perry et al. 2019). The following chain reaction (Eqs. 1–9) has been widely postulated as the possible mechanistic pathway for degrading dyes (Chauhan et al. 2019).

$$\text{Photoexcitation}: \text{Photocatalyst} + h\nu \rightarrow h^+ + e^- \quad (1)$$

$$O_2 \text{ ionosorption}: (O_2)_{ads} + e^- \rightarrow O_2^{\bullet -} \quad (2)$$

$$\text{Ionization of } H_2O: H_2O \rightleftharpoons H^+ + OH^- \quad (3)$$

$$\text{Superoxide gets protonated}: O_2^{\bullet-} + H^+ \rightarrow HOO^{\bullet} \quad (4)$$

$$\text{Formation of hydrogen peroxide}: 2HO_2^{\bullet} \rightarrow H_2O_2 + O_2 \quad (5)$$

$$\text{Formation of hydroxyl radical}: H_2O_2 + e^- \rightarrow HO^{\bullet} + OH^- \quad (6)$$

$$OH^- + h^+ \rightarrow HO^{\bullet} \quad (7)$$

Degradation of organic dye:

$$HO^{\bullet} + MB/\text{Industrial dye} \rightarrow CO_2 + H_2O + \text{degraded product} \quad (8)$$

$$\text{dye} + h^+ \rightarrow \text{dye}^{\bullet+} \rightarrow \text{oxidation of dye} \quad (9)$$

Furthermore, compared to traditional photocatalyst materials, nanosized catalysts have higher photocatalytic efficiency (Hariharan 2006; Ye et al. 2010a). This is because of the following two reasons:

a. **Quantum size effect:** Among the most immediate impacts occurs when the particle size falls below a specific critical limit (i.e., when the size decreases to the nanoscale range), resulting in quantum confinement (Kivrak et al. 2021). Depending on the material structure's size, the semiconductor's VB and CB transform into separate energy levels, which indicates that the valence band electric potential shifts more positively; alternatively, the electric potential of CB shifts more negatively (Einert et al. 2021). The oxidation–reduction potential of electron and hole is thus raised, resulting in higher oxidation activity of nanoscale photocatalysts (for instance, ZnO and TiO_2) (Colmenares et al. 2009).
b. **Higher specific surface area:** The adsorption ability of photocatalysts towards organic contaminants increases when more atoms are present on the surface. The activity is determined by how long it takes electrons and holes to get to the particle's surface. When particles are in the nanoscale range, their diameter becomes extremely small, making it much easier for charge carriers to move from the interior to the surface and initiate the redox reaction (Wang et al. 2018; Maity et al. 2022). The smaller the particle diameter, the greater will be surface to volume ratio, and the smaller will be the time interval that is utilized by the charge carriers diffusing to the surface from inside. It reduces the likelihood of electron–hole recombination. As a result, the photocatalytic activity can be improved. For example, the photocatalytic efficiency of nano-sized TiO_2 and ZnO is higher than that of conventional (bulk) TiO_2 and ZnO (Lin et al. 2006; Kim and Kwak 2007) (Table 2).

Photocatalytic reduction of heavy metal ions to their less toxic form

Reduction of Cr(VI) ion to Cr(III) ion by nitrogen-sulfur and carbon multi-doped (NSC) -TiO_2

Because of its prominent role in industrial contamination and toxicity to living beings, Cr has piqued the attention of scholars (Mills et al. 1996). Electroplating, leather tannery, mining, pigments refining of contaminated materials, and industries that manufacture chromate are the primary sources that release Cr(VI) into an aqueous solution (Lozano et al. 1992; Suksabye et al. 2007). Cr(III) and Cr(VI) are two oxidation states of chromium. According to Kowalski et al., Cr(VI) has hundreds of more detrimental consequences than Cr(III) (Giménez et al. 1996; Harish et al. 2012). Furthermore, Cr(VI) is versatile because of its weak absorption in inorganic areas.

In contrast, Cr(III) is smooth precipitating at close to neutral pH level and is less versatile in the environment due to its compassionate nature. Butler et al. found that Cr(VI) from CrO_4^{2-} dissolves more quickly in H_2O than CrIII (Butler and Davis 1993). Lin and his co-workers have reported various methods for removing Cr, such as reversible osmosis, precipitation, adsorption activities, photocatalysis, and ion transfer. But all of these strategies necessitated excessive resources and are not suitable for smaller organizations (Chenthamarakshan et al. 2000; Lee et al. 2006). Compared to other treatment procedures, photocatalytic degradation has gained the great attention of scholars. It is because of its unique and promising approach to solve environmental problems. In addition, it possesses high yield, durability, low cost, and applicability for redox reactions of harmful pollutants. It is well known that an aqueous solution containing Cr(IV) ions causes teratogenic, carcinogenic, and mutagenic effects on specific organisms (Luo et al. 2011; Giannakas et al. 2013; Zhang et al. 2013; Lei et al. 2014; Sun et al. 2014; Wang et al. 2014).

Table 2 Bandgap energies of some common semiconductor materials at 0 K (Sobczyński and Dobosz 2001; Thiruvenkatachari et al. 2008)

Semiconductors	CdS	Cu_2O	CdSe	TiO_2	ZnO	Fe_2O_3	PbS	ZnS	SnO_2	ZrO_2	WO_3	PbSe	Diamond
Bandgap energy	2.42	2.17	1.7	3.03	3.36	2.3	0.286	3.6	3.54	3.87	2.76	0.165	5.4

Especially, TiO_2 has received significant attention from researchers in comparison to other semiconductors, because of its higher stability, promising chemical characteristics, and relatively low cost (Fujishima et al. 2000). During the photolysis of TiO_2, electron–hole pairs are generated, and these photogenerated electron–hole pairs either recombine or participate in redox processes. Lei et al. described the fabrication of multi-doped NSC-TiO_2 *via* the sol–gel route in cooperation with the high-energy ball milling treatment (Lei et al. 2015). The NSC-TiO_2 was calcined at temperature 400, 500, 600, and 700 °C. $Ti(OBu)_4$ ($Bu = CH_2CH_2CH_2CH_3$) was used as a source of Ti and $SC(NH_2)_2$ as the doping agent. Multi-doped NSC-$TiO_{2\text{-}500}$ material resulted in a rapid decrease in the concentration of Cr(VI) under visible light illumination due to photocatalytic reduction. Absorption of photons, crystalline phase, crystal size, rate of separation of electron–hole pairs, and degree of crystallinity of the samples are quite often thought to be the main factors on which the photolytic activity depends. Hence, NSC-$TiO_{2\text{-}500}$ showed the maximum photocatalytic reduction ability for Cr(VI) in visible irradiations. This could be associated with the synergistic impact of (C, N, and S) multi-doping and enhanced anatase crystallization. The photocatalytic treatment of polluted water using nonmetal doped TiO_2 has shown great promise as a renewable water treatment method. Additionally, it is supposed to be an environmentally friendly alternative to photocatalytic treatment of contaminated water using metal-doped TiO_2. The latter is susceptible to potential metal problems and photo corrosion (Zhang et al. 2014).

Photocatalytic degradation of dye wastewater

Industrial chemicals, organic dyes, domestic wastes, and fertilizers are the main factors that contaminate the water, and now, this has become one of the worldwide environmental concerns. The textiles, paper manufacturing, cosmetics, and leather industries use organic dyes. Around one million tons of organic dyes have been produced worldwide annually (Erfani and Javanbakht 2018). Often, the wastewater from these industries has been released into the natural water sources without any pre-treatment. This dye-wastewater being non-biodegradable, pigmented, highly hazardous, and carcinogenic, when combined with natural water, affects the color of the water and may lead to severe diseases if used even in little amounts. Therefore, it is the need of the hour to have advanced, reliable, and efficient techniques for treating dye wastewater. Generally, coagulation and adsorption are conventional methods for treating wastewater polluted by dyes (Regkouzas and Diamadopoulos 2019; Campinas et al. 2021). But these methods have many drawbacks, such as the pollutant is not eradicated and the production of sludge that needs post-treatment disposal. Therefore, the purification of dye-contaminated wastewater needs advanced methods of treatment. Furthermore, the dye-contaminated wastewater contains toxic, nonbiodegradable molecules and intensively conjugated structural species that are hazardous to humans and the environment (Rojviroon et al. 2015; Al-Mamun et al. 2019; Ekka et al. 2019; Bagheri et al. 2020).

Recently, photocatalysts have gained attention owing to their efficient and promising water purification abilities. The photocatalytic treatment of the dye-wastewater comprises a chemical reaction between contaminants and photocatalysts. Photocatalytic degradation of the dyes at room temperature takes just a few hours. After the photocatalytic degradation, the pollutants are degraded to less harmful species (CO_2 and H_2O) without producing any secondary toxic products. ZnO, TiO_2, SiO_2, and CeO_2 are metal oxide semiconductors generally used as photocatalysts (Khan et al. 2015).

Factors affecting the photocatalytic degradation of dye wastewater

(i) Light source effects

With increasing exposure to light intensity, the percentage breakdown of dyes in wastewater is higher. At higher light intensity, the enhancement is noticeable because the electron–hole production is predominant at high irradiation intensity thus the chance of electron–hole recombination is meager (Ji et al. 2022; Zhu et al. 2022). Conversely, when the intensity of the irradiation light is low, electron–hole pair detachment competes with recombination, which reduces the generation of free radicals, resulting in a lower percentage of dye degradation (Alhakimi et al. 2003; Choi et al. 1994; Kuang et al. 2008).

Most photocatalytic degradation research has been done at wavelengths between 320 and 380 nm, corresponding to the bandgap energy of the ZnO and TiO_2 photocatalysts (Mandor et al. 2022). As a result, solar irradiation or artificial lamps can be used to provide the requisite radiation field. Radiation (wavelength range of 320–380 nm) is delivered in a conventional photocatalytic reactor by fluorescent low-pressure and medium mercury lamps providing low and high-intensity UV light, respectively, in the short, medium, and long UV spectrum (Thiruvenkatachari et al. 2008).

(ii) pH effects

Because the pH impacts the adsorption of contaminants at the photocatalysts' surface, the aqueous solution's pH level is a crucial aspect of photocatalytic degradation of dye and wastewater. Pharmaceutical, dairy, and textiles sectors produce a wide pH range of wastewater. Furthermore, the pH of the solution also influences the production of $^{\bullet}OH$ radicals, which is required for photocatalytic reactions (Lawless et al. 1991). Consequently, pH has a crucial role in the formation of $^{\bullet}OH$ as well as in the chemical composition of wastes. Therefore, numerous attempts have been made to examine

the role of pH in wastewater deterioration under ultraviolet and solar irradiation (Zhu et al. 2005). For all three (neutral, cationic, and anionic) dyes in wastewater, photocatalytic degradation has been examined at pH levels in the range of 3 (acidic) to 13 (alkaline). The breakdown efficiency of several azo dye wastes was decreased at an optimal dye concentration in both acidic and alkaline (Konstantinou and Albanis 2004). It was examined that some non-biodegradable cationic dyes such as MB, rhodamine B (RhB), and MG degraded the least efficient in the presence of H_2O_2 at both acidic and alkaline pH levels but degraded the most effectively at neutral pH value (Cheng et al. 2004). The inhibitory effect was more prominent in the high alkaline range (pH 11–13). The $^{\bullet}OH$ radicals are removed so rapidly at high pH values that they would not have enough time to react with dyes present in the wastewater. For instance, pH influences the surface of TiO_2 and ZnO photocatalysts, the breakdown of organic contaminants (or dyes in wastewater), and the generation of $^{\bullet}OH$ radicals (Balcioğlu and Inel 1996).

The photocatalysts' zero charges (pzc) point can explain the increased photodegradation performance at neutral pH. Correspondingly, for TiO_2 and ZnO, the pzc value was observed at pH 6.25170 and 8.9174. In alkaline media (pH > pzc), photocatalyst surfaces get negatively charged; however, in acid media (pH < pzc), they get positively charged. Though TiO_2 and ZnO have an amphoteric nature with a zero charge in the pH range near their pzc value, dye pollutants adsorb exceedingly well at that pH value, hence increased photodegradation performance was expected at that pH value (Cheng et al. 2004). As a result, the pH value substantially impacts the adsorption capacities at the photocatalyst surface, and therefore, photodegradation rates are negligible at extreme pH values (Balcioğlu and Inel 1996).

As a result, the pH value substantially impacts the adsorption capacities at the photocatalyst surface, and therefore, photodegradation rates are negligible at extreme pH values. Since there are 3 possible reaction pathways behind the organic pollutant/dye degradation reaction, i.e., oxidation and reduction by hole and electron, respectively, in semiconductor photocatalysts, and attack of $^{\bullet}OH$ radical, interpreting the impact of pH values on the performance of the degradation reaction is an insensitive piece of work. The relevance of each parameter is highly dependent on the substrate's nature and pH value. For organic dyes and pollutants, it is reasonable to assume that the principal reaction is regulated by $^{\bullet}OH$ attack, which is assisted by the large concentration of $^{\bullet}OH$ at pH values near neutral (Cheng et al. 2004). Another explanation for pH impacts is the ionic specification of organic dyes. The protonation or deprotonation of dyes can significantly influence their adsorption properties and oxidation–reduction activity (Konstantinou and Albanis 2004).

(iii) **Temperature and pollutant concentration**

For all kinds of catalysts, it was found that the decolorization of real textile industrial wastewater rises with time and temperature. Furthermore, the findings showed that a greater temperature facilitates the decomposition of contaminants in wastewater. It is most likely because the activation energy also increases when the operating temperature rises (Kumar 2017). The time it takes for wastewater to decompose is reduced when the dye (a contaminant in waste water) content is reduced. Although this industrial wastewater's content is relatively low than the original concentration, dye ions will likely expose the active catalyst sites. The increased dye concentration could also be accountable for screening the exposed light, reducing light intensity (Kiriakidou et al. 1999).

(iv) **Loading of photocatalyst**

The impact of several catalyst loadings on photocatalytic degradation of dye wastewater has been studied extensively (Konstantinou and Albanis 2004; Sun et al. 2008; Akpan and Hameed 2009). The initial degradation rates of azo dyes in an aqueous medium were precisely proportional to TiO_2 catalyst concentration, according to Konstantinou and colleagues for azo dye degradation by TiO_2-supported photocatalysis (Konstantinou and Albanis 2004). Remarkably, studies of UV-supported photocatalytic decomposition of industrial wastewater using various photocatalyst (ZnO, anatase, or rutile) loading showed that the optimum photocatalyst mass required for maximum decolourization efficiency is unaffected by exposure time, irradiation source, or pollutant characteristics (Hussein 2012).

(xxii) **Nature of catalysts**

TiO_2 is the most widely used photocatalyst while analyzing the effect of different prospective photocatalysts on their thermal and chemical activity, stability under various working environments, ease of access and ease of use in several physical forms, affordability, toxic effects, and environmental friendliness. Only rutile and anatase are well-established crystal forms among three crystal structures that could be employed as possible photocatalysts (Agustina et al. 2005). Pillai and his colleagues found that the photocatalytic characteristics of different phases of TiO_2 materials vary greatly, with rutile phases having the lowest photoactivity (Lindner et al. 1997; Pillai et al. 2007). The anatase phase of TiO_2 is a better photocatalyst than rutile, but the brookite phase has not been instigated much (Paola et al. 2013).

(vi) **Effect of the water matrices**

The water matrix also contributes significantly to the AOPs' capacity to remove pollutants (Hosseini et al. 2022). Dissolved and suspended components have a major impact

on the percentage removal in highly charged water. Dissolved materials, however, may affect the photocatalytic water disinfection process and have a variety of impacts, including positive, negative, or neutral ones (García-Fernández et al. 2015, 2019). If dissolved organic compounds are present in the aqueous matrix, scavengers may also prevent the removal of those materials (DOM). In neutral water, natural organic substances, carbonates, bromides, and bicarbonate can function as •OH scavengers. Additionally, the effectiveness of removing pollutants declines as water matrix complexity increases. When present in high concentrations in the wastewater, inorganic salts like NaCl, $FeCl_2$, $CaCl_2$, $FeCl_3$, and $AlCl_3$ that are present in the water matrix have a detrimental effect on photocatalytic reactions and can even completely stop these reactions (Real et al. 2010; Dimitroula et al. 2012; Rioja et al. 2016).

Photocatalytic degradation of dyes and bacterial inactivation from water

Ti-based nanomaterials

TiO_2 nanotubes photocatalyst has many advantages, such as the high ratio of surface area to volume, numerous active sites, low cost of synthesis, and good photo-adsorption (Sopha et al. 2017; Viet et al. 2018; Parnicka et al. 2019; Hu et al. 2020). RB5 and IC dyes are reactive and acid groups. The molecular structures of RB5 and IC dyes contain amine groups and sulfonic acid on the aromatic rings, respectively. These dyes having such complex structures prevent the growth of microorganisms and therefore restrain their elimination capabilities (Li et al. 2018a; Bagheri et al. 2020). Rojviroon et al. reported the photocatalytic decolorization of RB5 and IC dyes by TiO_2 nanotubes synthesized *via* electrochemical anodization (Rojviroon et al. 2021).

The increase in the depth and the diameter of the TiO_2 nanotubes with increasing anodization voltage suggests the increased photocatalytic degradation efficiency for dye wastewater with the increase in surface area of the catalyst. Now, a greater number of dye molecules can be adsorbed and catalyzed. Hence, with the increasing anodization, the decolorization efficiency of the TiO_2 nanotubes for these dyes increases. The improved physical features of the TiO_2 nanotubes, such as the inner diameter, wall thickness, and depth, were attributed to the increased decolorization efficiency. The tubular-structured network of TiO_2 nanotubes got more symmetrically spaced and spread across a greater surface area as the voltage applied during anodization increased. It raised the electron transfer potential and ion habitation on the active sites of the TiO_2 nanotube sheets when illuminated with UVA light (Gao et al. 2018; Li et al. 2018b; Suhaimy et al. 2018). In addition, electrochemical anodization led to a nanotube array structure with more active sites. These active sites adsorbed and captured dye molecules on the nanotube surface, allowing electrons in the VB to transfer in parallel and vertically. It raised photon efficiency while lowering electron–hole pair recombination (Gao et al. 2018; Li et al. 2020a). With increasing initial dye concentrations (for both dyes), the decolorization efficiency of TiO_2 nanotube photocatalyst (anodized at all voltages) was reduced. This is because the higher concentration of dye caused inhibitory effects, preventing the light from reaching at the active sites over the surface of the photocatalyst. Specifically, the development of $^{\bullet}OH$ radicals and $O_2^{\bullet-}$ radicals on the active sites was prevented by greater dye concentrations (Anwer et al. 2019; Fatima et al. 2019; Li et al. 2020b). In addition, the decolorization efficiency also depends upon the extent of the dye molecules' complexity in their structures (Kumar et al. 2017a; Natarajan et al. 2018; Neena et al. 2018; Lu et al. 2020).

The photocatalyst's ability to decolorize reactive oxidant species was reduced. Over time, dissolved organic matter (DOM) aggregation occurred on the photocatalyst surface and inhibited the active sites (Ye et al. 2018). Some intermediate species in treated wastewater are harmful and poisonous, regardless of their lighter appearance. Consequently, if present in higher concentrations, it may threaten humans and aquatic creatures (Pirkarami et al. 2014; Rasheed et al. 2017). Jafri et al. described the photodegradation of the MB dye by TiO_2 hollow nano-fiber (Jafri et al. 2021). First, TiO_2 hollow nanofibers having desired characteristics were fabricated by template synthesis. Then, polyacrylonitrile was employed as a template, and the dip-coating technique settled down the TiO_2 precursor. Afterwards, the influence of variation in calcination temperature in the course of template removal on the fiber characteristics was studied.

The photocatalytic degradation test exhibited MB dye degradation in an aqueous solution depending on the irradiation time using the catalysts THNF400, THNF500, and THNF600. The degradation percentage of MB dye was 42.9%, 61.7%, and 85.5%, respectively. THNF600 exceeded THNF400 and THNF500 in terms of photocatalytic performance. When it comes to photocatalyst qualities, THNF600's outstanding performance can be attributed to (i) increased surface area for UV irradiation and adsorption of contaminant molecule; (ii) the heterojunctions amid the anatase and rutile phases lead to rapid electron–hole separations (iii) light scattering impact in hollow nanofibers leads to efficient light utilization as shown in Fig. 7a. From this, we can deduce that using a photocatalyst enforces the degradation of MB dye.

The active sites of the photocatalyst increase in the presence of the greater amount of photocatalysts, increasing the number of photons absorbed and the probability of $^{\bullet}OH$ radical formation, allowing a greater number of MB dye

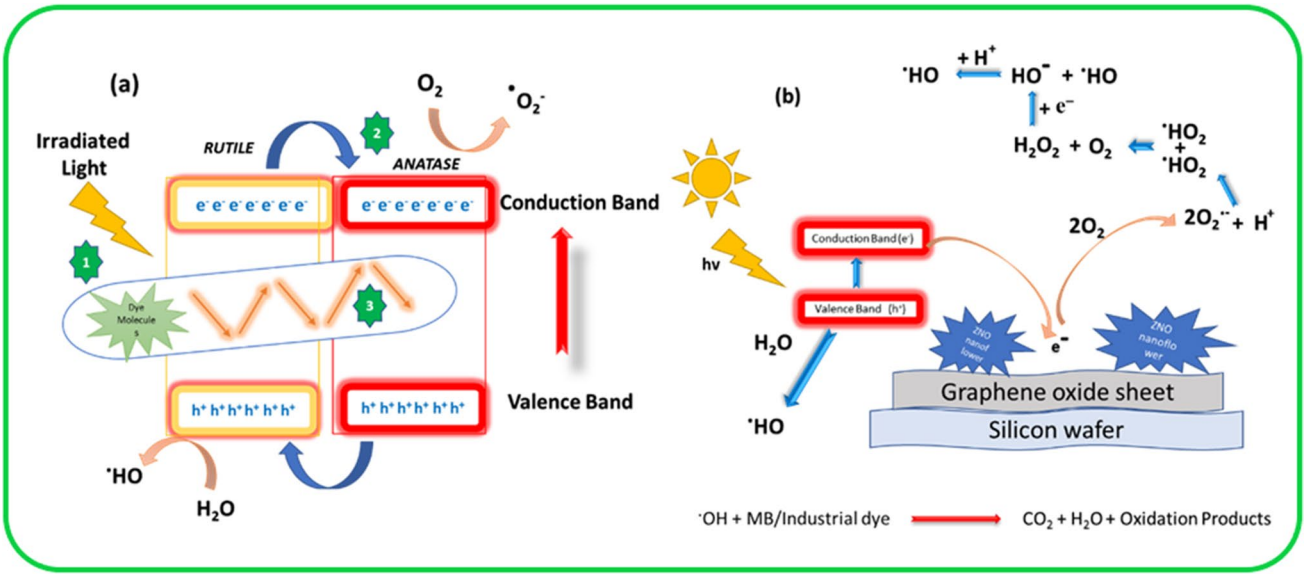

Fig. 7 **a** TiO_2 hollow nanofibers with increased photocatalytic characteristics. (1) The extra surface for molecule adsorption produced by the inner core and outside shell, (2) heterojunction formed by mixed-phase photocatalyst, and (3) light scattering effect inside the nanofiber interior, **b** diagram depicting the decolorisation of MB/industrial dye utilizing ZnO/GO nanocomposite as a photocatalyst in the presence of sunlight (Chauhan et al. 2019) (Jafri et al. 2021)

molecules to be mineralized (Yunus et al. 2017). The number of pollutant molecules adsorbed on the surface of the photocatalyst varies directly with their concentration which further causes the aggregation of contaminants and competition for active sites. The irradiated UV light is primarily absorbed by contaminant molecules rather than catalysts, resulting in decreased •OH radical generation. As a result, as the concentration of MB dye increases, the number of free radicals attacking the dye molecules reduces. Therefore, a greater extent of catalyst loading is needed for degrading higher doses of MB dye (Siddique et al. 2014).

However, while using high concentrations of TiO_2 particles, the scattering of light is a practical limitation. Therefore, the degradation rate will drop due to reduced photonic flux within the irradiated solution (Chen et al. 2007). In addition, the competition for adsorption by OH^- on the same sites reduced, leading to a lower generation rate of •OH radical, the primary oxidant required for a greater degree of degradation. Consequently, the photocatalytic degradation rate became slower (Chen et al. 2007).

Rtimi et al. reported a novel approach for the decoloration of MB dye in the presence of low-intensity solar simulated light using polyethylene-TiO_2 (PE-TiO_2) thin film (Rtimi et al. 2015). It was noticed that the decoloration of MB dye became faster with an increase in the TiO_2 loading. The proposed reaction mechanism involves the generation of a short-lived unstable cation from generated MB* excited state upon light irradiation. This unstable cation then breaks down and simultaneously introduces an electron onto TiO_2. This electron either interacts with the O_2 in the solution or is transported to the adsorbed O_2 on the TiO_2 surface, producing $O_2^{\bullet}-$ and other highly oxidative radicals. The following reaction is proposed for the formation of MB^+ (Mills 2012):

$$\begin{aligned} MB{+}PE - TiO_2 + solarlight \rightarrow [MB^* \ldots\ldots TiO_2] \\ PE \rightarrow MB^+ + [PE - TiO_2 + e^-] \end{aligned} \quad (10)$$

The intensity and wavelength of the lamp were found to have a significant impact on MB decoloration. Under optimum conditions, 98% of MB dye decoloration has been reported (Rtimi et al. 2015).

For the first time, Rtimi and his colleagues described the formation of adhesive, uniform TiO_2 layers photocatalyst produced by HIPIMS and DCMS. The fabricated PE-TiO_2 films have distinct particle size, compactness, optical, and redox properties (Rtimi et al. 2016). When compared to HIPIMS samples, the levels of Ti-ions found to have been leached out during disinfection were greater in the DCMS samples. Compared to DCMS samples, bacterial inactivation occurred on HIPIMS samples nearly 3 times faster. By the investigation of pH, it was determined that hydroperoxide ($HO_2^{\bullet}$ and O_2^-) produced on the PE-TiO_2 surface indirectly contributed to the inactivation of the bacteria. During the process of bacterial inactivation, the surface •OH—radicals were statistically controlled as a function of temperature and time (Rtimi et al. 2016). The deconvolution for the XPS DCMS PE-TiO_2 peak prior to bacterial inactivation is depicted in Fig. 8a. Figure 8b depicts the redox process for

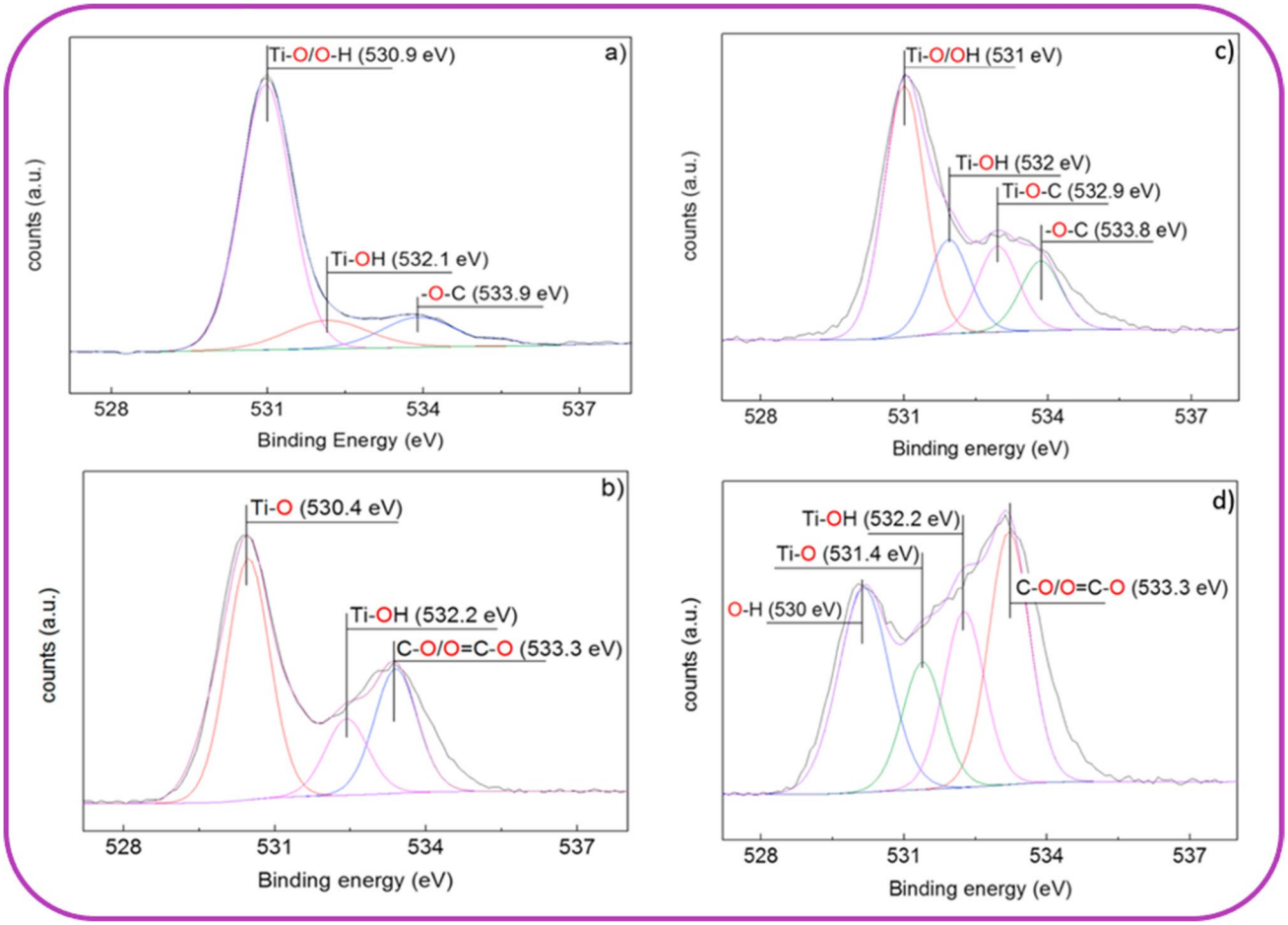

Fig. 8 O1s peak deconvolution of PE-TiO_2 samples pre-treated with RF plasma for 15 min and 8 min of DCMS sputtering: **a** before bacterial inactivation, **b** after bacterial inactivation, and 4 min of HIPIMS sputtering: **c** before bacterial inactivation, **d** after bacterial inactivation. Reproduced with permission, copyright © 2020 Elsevier Ltd, (licence number — 5,350,891,329,689). All rights reserved (Rtimi et al. 2016)

the Ti–O species going through a binding energy (BE) shift from 530.9 to 530.4 eV following bacterial inactivation. This is an indication of a decline in the (O1s)-species. The—C-O peak, which had a BE of 533.9 eV before bacterial inactivation, decreased to 533.3 eV concurrent with bacterial oxidation. In contrast to the counts reported for the DCMS sputtered samples in Fig. 8a and b, HIPIMS reveals a greater number of XPS-counts for O1s species on the PE-TiO_2 films both before and after bacterial disinfection as shown in Figs. 8c and 8d. The change in the XPS deconvoluted peaks also reflects the redox reactions of the surface species.

Zeghioud and his colleagues reported the degradation of RG12 dye in an aqueous medium by TiO_2 impregnated polyester at room temperature (Zeghioud et al. 2017). Utilizing distinct polyester pretreatments (plasma surface activation and UV-C photons), the TiO_2 loading on polyester was enhanced. The study of both catalysts revealed that radio-frequency plasma pretreatment polyester had no photocatalytic activity under visible light and had significantly less activity than UVC-pretreated-impregnated materials under UV light. Within 120 min of optimal operating circumstances, RG12 was removed entirely (100%) under UV light and 87.14% under visible light. Furthermore, the addition of H_2O_2 had a favorable impact on the degradation, i.e., the period of complete degradation of dye was reduced to 80 min when exposed to UV light. Over five reuse cycles, the photo-catalyst maintained its photocatalytic activity and showed remarkable stability (Zeghioud et al. 2017).

In another experimental study, Zeghioud and his colleagues also reported the degradation of RG12 dye by Cu_xO/TiO_2 photocatalyst fabricated via HiPIMS, in the presence of visible light-emitting diodes (LEDs) illumination (Zeghioud et al. 2019). The fabrication of photocatalyst was optimized by varying different parameters. The photocatalyst fabricated at 40 A in HiPIMS mode was found to have the highest RG12 degradation efficiency. In addition, it was noticed that $K_2S_2O_8$ and H_2O_2 addition improved the photocatalytic efficiency by 6 and 7 times correspondingly. While the

addition of Cu and NaCl salt significantly reduced the rate of RG12 decoloration by 4 and 2 times, likewise (Zeghioud et al. 2019).

Nesic and his colleagues observed the bacterial inhibition (*Escherichia coli*) on TiO_2-polyester (TiO_2-PES) in both the absence and presence of light irradiation (Nesic et al. 2014). With a greater TiO_2 loading on the PES, up to 5%, it was noticed that the bacterial inhibition increased. On a TiO_2-PES 5% TiO_2 sample, the TiO_2 accumulates and interacts with the *E. coli* cell in darkness, completely removing bacterial cultivability within 2 h. It was noticed that bacterial disinfection on TiO_2-PES in the dark took a longer time than disinfection under low-intensity simulated solar irradiation. On TiO_2-PES samples, photocatalysis by TiO_2 NPs resulted in 100% loss in bacterial viability in 60-min. The ROS generated under light due to the NP's radical production is thought to be the cause of the oxidative stress that caused the shorter bacterial reduction time under light irradiation (Nesic et al. 2014).

Bonnefond and his colleagues reported that the bacterial (*Escherichia coli*) inactivation pickering stabilized hybrid acrylic/TiO_2 latex films under low-intensity simulated solar light irradiation (Bonnefond et al. 2015). No bacterial inactivation was reported under dark circumstances. Photocatalytic efficiencies of the films were examined using two different TiO_2 loadings. The films containing 10 weight based on monomers (wbm)% and 20 wbm% of TiO_2 showed 100% bacterial inactivation in 2 and 6 h respectively. The hybrid films demonstrated the repeated inactivation of *Escherichia coli* in the presence of solar irradiation. Because the acrylic/TiO_2 hybrid film is rougher than a new film, it positively impacts the inactivation of *E. coli* (Bonnefond et al. 2015).

Ti-based magnetic photocatalyst

2,4-DCP is a widespread organic non-biodegradable pollutant in drinking and waste water. It has a long history of use as preservatives, herbicides, insecticides, and germicides (Sabhi and Kiwi 2001; Zanjanchi et al. 2010). Cancers linked to the endocrine system are also caused by it (Chen et al. 2017). Yu et al. reported the photocatalytic degradation of 2,4-DCP using the magnetically separable TiO_2/FeO_x microstructure decorated with POM (Yu et al. 2019c). Under simulated solar light at pH 5.0, non-magnetic TiO_2/POM(1%) led to the fastest 2,4-DCP degradation rates with 87.6%, while magnetically separable TiO_2/FeO_x(25%)/POM(1%) led to 76.6% 2,4-DCP degradation within 3 h (Yu et al. 2019c). TiO_2/FeO_x(25%)/POM (1%) can be separated magnetically. Hence, the separation of photocatalysts becomes easy and less costly.

Dabirvaziri et al. reported the fabrication of γ-Fe_2O_3@SiO_2@TiO_2–Ag magnetically separable photocatalyst using a combination of co-precipitation, sol–gel, and photo-deposition techniques (Dabirvaziri et al. 2019). It was reported that about 94% of Basic blue 41 dye was decomposed within 3 h in the presence of UV light by γ-Fe_2O_3@SiO_2@TiO_2–Ag while only 63% of the same dye was decomposed by pure γ-Fe_2O_3@SiO_2@TiO_2. The magnetic responsive properties of the as-prepared superparamagnetic photocatalyst allow for rapid catalyst separation, recycling from the reaction medium, and reuse in subsequent reactions. No significant reduction in the photocatalytic activity was noticed even after five consecutive cycles which indicated its good stability. Additional antibacterial tests showed that the -Fe_2O_3@SiO_2@TiO_2-Ag has outstanding antibacterial activity under visible light conditions against two separate bacterial strains (*E. coli* and *S. aureus*). In addition, it was reported that -Fe_2O_3@SiO_2@TiO_2-Ag had significantly greater antibacterial activity than pure Fe_2O_3@SiO_2@TiO_2 particles (Dabirvaziri et al. 2019). Jahanara and Farhadi reported the synthesis of magnetic cadmium titanate–copper ferrite ($CdTiO_3/CuFe_2O_4$) nanocomposite *via* a sol–gel hydrothermal method (Jahanara and Farhadi 2019). The photocatalytic performance of this $CdTiO_3$-based magnetic nanocomposite was examined for degradation of organic dye pollutants dyes like MB, RhB, and MO in the presence of hydrogen peroxide and visible light. The outcomes demonstrated that three dyes were totally degraded by the photocatalyst within 90–100 min. The heterogeneous $CdTiO_3/CuFe_2O_4$ nanocomposite showed noticeably improved photocatalytic activity in comparison to pure $CdTiO_3$ and $CuFe_2O_4$ (Jahanara and Farhadi 2019). Due to its magnetic characteristics, the $CdTiO_3/CuFe_2O_4$ can be magnetically separated. To examine the stability of the $CdTiO_3/CuFe_2O_4$ nanocomposite, it was used three times for the photodegradation of MB. After three recycles, the catalyst activity exhibited no discernible change.

Chen et al. fabricated ternary $CaTiO_3$/reduced graphene oxide (rGO)/$NiFe_2O_4$ nanocomposite *via* polyacrylamide gel and hydrothermal process (Chen et al. 2019). The photocatalytic performance of this nanocomposite was assessed through the degradation of MB and RhB under the effect of simulated sunlight irradiation. It was observed that when compared to pure $CaTiO_3$ and $NiFe_2O_4$, the ternary nanocomposite exhibited noticeably improved photocatalytic activity. When exposed to radiation for 180 min, MB dye was degraded approximately 11 and 38% by bare $NiFe_2O_4$ and $CaTiO_3$, respectively, while RhB degraded nearly 10 and 31% for pure $NiFe_2O_4$ and $CaTiO_3$, respectively. Contrarily, under the same conditions, $CaTiO_3$/rGO/$NiFe_2O_4$ nanocomposite degraded almost 83% of MB and 74% of RhB, respectively (Chen et al. 2019). Additionally, the nanocomposite demonstrated ferromagnetism and is easily recovered by an outside magnetic field. The recycling photocatalytic experiment showed that the nanocomposite has good reusability in the photocatalytic process. Esania et al. reported the

synthesis of a novel ZnO-Fe_3O_4/TiO_2 nanocomposite using a combination of solvo-hydrothermal and sol–gel routes. This nanocomposite showed photocatalytic removal of Reactive Blue 21 (RB21) in the presence of UV light. Under optimum conditions, 99% photocatalytic decoloration of RB21 was observed. Additionally, after five consecutive catalytic cycles, the RB21 decoloration efficiency with ZnO-Fe_3O_4/TiO_2 nanocomposite was reported to be 97.10% of its initial photocatalytic activity from 99.89% (Esania et al. 2022). As a result, the photocatalyst was fairly stable. An improved Pechini sol–gel process was used by Tatarchuk et al. to fabricate the $CoFe_2O_4$@TiO_2 magnetic nanocomposite. In comparison to TiO_2 and $CoFe_2O_4$ alone, the $CoFe_2O_4$@TiO_2 nanocomposite was shown to have an adsorption efficiency that was more than twice as high (Tatarchuk et al. 2020). Only the production of distorted titania nanocrystals is responsible for the observed synergistic impact. The magnetic nanoadsorbent was found to be effective at removing dichromate anions (83% removal efficiency) and Congo red dye (61% removal efficiency) from water (Tatarchuk et al. 2020).

Zinc-based nanomaterials

Chauhan et al. used ZnO/GO composite consistently produced over silicon substrate to describe an alternative and novel method for decolorizing MB dye ((Chauhan et al. 2019). The photo-excitation of electrons (existing at the surface of ZnO) occurs when ZnO/GO (zinc oxide/graphene oxide) is exposed to sunlight. Electrons from the VB of ZnO are transported to the CB of ZnO, creating a hole in the VB (Chauhan et al. 2019). The reduced work function of GO helps in effective electron interaction between GO and ZnO, resulting in electron scavenging from ZnO's CB to GO. With the help of GO, this process starts with electron–hole pair separation in ZnO. GO is a suitable electron acceptor with a 2-D-conjugated nanostructure that effectively eliminates electron–hole recombination losses caused by the bandgap of ZnO (Houas et al. 2001). As a result, charge separation improves the photocatalytic efficiency of the system. Reactive oxyradicals such as $O_2^{\bullet}$ and $^{\bullet}OH$/$^{\bullet}OOH$ are formed when photo-excited electron interacts with surface oxygen species and H_2O molecules. While holes in the VB of zinc oxide interact with water molecules to produce the free $^{\bullet}OH$ radicals (Gnaser et al. 2005). These $^{\bullet}OH$ radicals are highly reactive oxidants that break down dyes rapidly into less harmful compounds. Equations (11)–(20) outline the possible processes that occur during dye decolourization and are depicted schematically in Fig. 7b (An et al. 2014). According to the dark adsorption investigation, the ZnO/GO nanocomposite adsorbs a little fraction of dye, whereas the absorption of dye on the surface of ZnO is negligible. The attractive electrostatic force amid the negative dipole functional (oxygen groups) groups of GO sheets and the positive dipole group of MB dye ($=N^+ H^-$) promotes dye molecule adsorption (Sharma et al. 2013). As a result, in the case of ZnO/GO nanocomposite material, adsorption somewhat facilitates photocatalysis.

$$ZnO + hv \rightarrow \mathrm{ZnO}\left(\mathrm{h}^+ + e^-\right) \tag{11}$$

$$GO + e^- \rightarrow GO(e^-) \tag{12}$$

$$(O_2)_{ads} + GO(e^-) \rightarrow O_2^{\bullet -} + GO \tag{13}$$

$$H_2O \rightleftharpoons \mathrm{H}^+ + OH^- \tag{14}$$

$$O_2^{\bullet -} + \mathrm{H}^+ \rightarrow HOO^{\bullet} \tag{15}$$

$$2HO_2^{\bullet} \rightarrow H_2O_2 + O_2 \tag{16}$$

$$H_2O_2 + e^- \rightarrow HO^{\bullet} + OH^- \tag{17}$$

$$OH^- + \mathrm{h}^+ \rightarrow HO^{\bullet} \tag{18}$$

$$HO^{\bullet} + MB/\text{Industrial dye} \rightarrow CO_2 + H_2O + \text{degraded product} \tag{19}$$

$$\text{dye} + \mathrm{h}^+ \rightarrow dye^{\bullet +} \rightarrow \text{oxidation of dye} \tag{20}$$

The drop-in dye concentration is called dye decolorization and is the result of dye oxidation in the vicinity of $^{\bullet}OH$ radicals. Under the same operating circumstances, the pure ZnO catalyst degrades MB dye by 66% while the ZnO/GO catalyst by 99% in just 1 h. The inclusion of the GO sheet enhances the surface and electrical characteristics of ZnO. The addition of GO improved charge transfer, reduced band gap, boosted surface oxygen species, and enhanced the light-absorbing capability of the ZnO/GO nanocomposite (Chauhan et al. 2019). Figure 9 represents the photocatalytic reaction kinetic for degradation of MB dye.

Yu et al. reported the sulfamethazine (SMT) degradation utilizing ZnO/Cu_xO hexagonal nanowires under the effect of solar and visible light (Yu et al. 2019a). A faster SMT-degradation rate was observed when the photocatalyst with composition ZnO/$Cu_{x=1.25}O$ was used. The type of light employed affects the interfacial charge transfer (IFCT) between ZnO and Cu_xO (solar or visible light). A twofold mechanistic route was reported leading to SMT degradation under visible or solar irradiation. It has been noted that CuO doping reduces the ZnO band gap. The extent of SMT degradation was found to increase with the intensity of light employed. The photocatalyst exhibits semiconductor behavior in the course of SMT breakdown. The two primary radicals causing SMT breakdown were reported to be

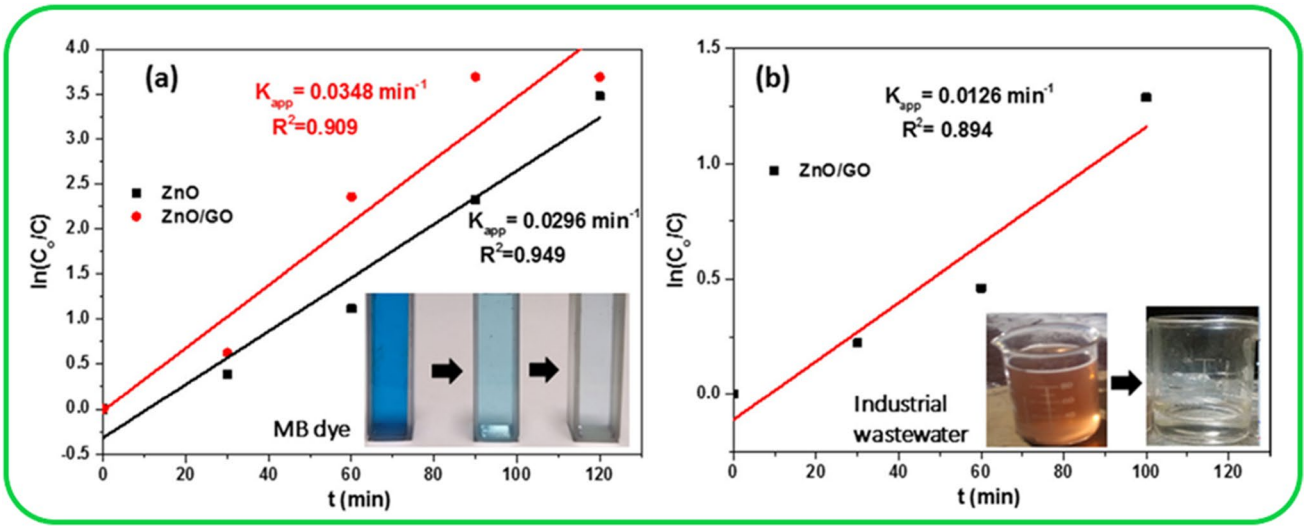

Fig. 9 **a** Photocatalytic reaction kinetic study of MB dye utilizing pure ZnO and ZnO/GO catalyst, and **b** steady degradation of MB dye by ZnO/GO catalyst as a function of irradiation time. Reproduced with permission, copyright © 2020 Elsevier Ltd, (licence number — 5,292,381,016,579). All rights reserved (Chauhan et al. 2019)

valence band hole and •OH-radicals. When benzoquinone was introduced as an HO_2/$^{\bullet}O_2^-$ scavenger, the SMT degradation was reduced by 20%. The SMT degradation rates are slower under visible light irradiation than those attained in the presence of solar light. The quickest SMT deterioration was seen with the ZnO/$Cu_{x=1.25}O$ sample (Yu et al. 2019a).

Biomass-derived ZnS and CdS photocatalysts

Green fabrication of nanoparticles (NPs) is receiving significant attention as a novel nanobiotechnology approach for synthesizing economic, environment-friendly, and high stability nanoparticles. Therefore, green fabrication has appeared as a better and safer substitute for existing methods. In recent years, bio-templates derived from natural sources such as plant extracts and microorganisms have been used to design complicated nanomaterials with large surface areas (Patete et al. 2011; Nakkala et al. 2015; Rao et al. 2016; Kumar et al. 2017b). Recently, photocatalysts such as metal sulfides were synthesized using chemical procedures that used hazardous reagents and required high temperatures and pressures. Therefore, many attempts have been devoted for developing safer and cleaner materials. The green approach for fabricating metal sulfides employing plants, bacteria, and fungi emphasizes zinc sulfide (ZnS) and cadmium sulfide (CdS) (Munyai and Hintsho-Mbita 2021). The catalytic performance of the *C. gigantea* leaf extract capped CdS NPs was verified by UV–vis absorption spectra, which was substantially superior to those of other photocatalysts including ZnO, TiO_2, WO_3, SnO_2, and Fe_2O_3. This could be owing to the –OH group-containing components of extract interacting directly. The activities of all the studies were examined to understand whether CdS NPs have greater photocatalytic activity. First, the VB electrons were excited by visible light irradiation to the CB, and holes in VB were created. The electrons and holes were then transported to the crystals' surfaces. They reacted with O_2 and water to generate $O_2^{\bullet-}$ and •OH, which serve as the active center and strong oxidizing agent for photocatalytic activity. The probable mechanistic pathway of EY and MB dyes photocatalytic reactions is similar to the mechanistic pathway explained in Eqs. (1)–(9) (Ayodhya and Veerabhadram 2017).

In the photodegradation of EY and MB dyes in the presence of solar irradiation, the degradation performances were measured with and without the use of fabricated *C. gigantea* leaf extract capped CdS NPs as shown in Fig. 10. It depicts the fluctuation in MB and EY dye degradation over the photocatalytic reaction in the presence of solar irradiation without and in the presence of CdS NPs. Interestingly, self-degradation of the MB (9.64%) and EY (14.72%) dyes was very low after 1 h of solar irradiation; on the other hand, the MB (85.53%) and EY (91.12%) dyes degraded exceedingly by using *C. gigantea* leaf extract capped CdS NPs after 1 h of solar irradiation (Ayodhya and Veerabhadram 2017).

ZnS semiconductor has a high-energy bandgap. It can be found sequentially in hexagonal wurtzite or cubic zinc blend structural forms. It has been demonstrated to have extensive applications such as biological sensors, light-emitting diodes (LEDs), and photocatalysts (Sorensen et al. 2006; Xiaosheng Fang et al. 2009; Chen et al. 2010; Zhu et al. 2011). Chemically synthesized ZnS nanoparticles and P25 (available commercially TiO_2 nanoparticles) were employed as control groups to investigate the photocatalytic performance of biologically synthesized

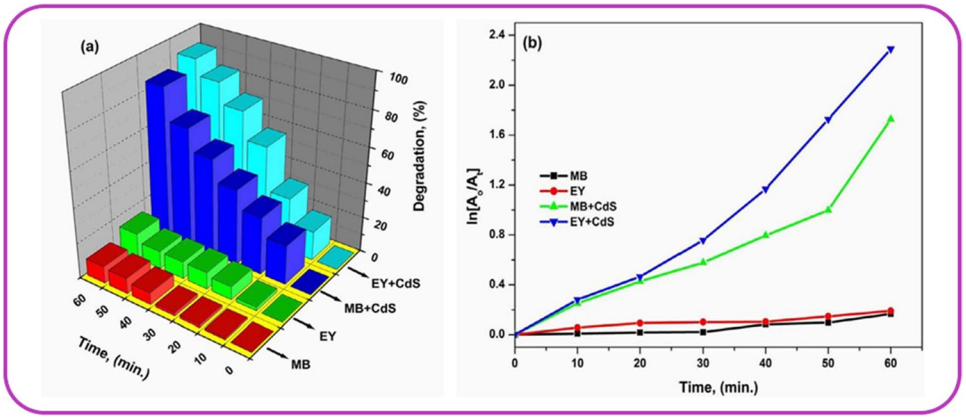

Fig. 10 **a** 3–D bar diagram of the degradation performances and **b** kinetic graphs of the photocatalytic degradation of MB and EY dyes without and with the use of fabricated *C. gigantea* leaf extract capped CdS NPs. Reproduced with permission, copyright © 2020 Elsevier Ltd, (licence number — 5,292,390,159,324). All rights reserved (Ayodhya and Veerabhadram 2017)

ZnS nanoparticles. Biosynthesized ZnS, chemically synthesized ZnS, and P25, on the other flip, all work well in MB photodegradation. Biosynthesized ZnS has the highest photocatalytic performance, degrading 96% of MB in 120 min of UV light exposure (Chen et al. 2016a).

A straightforward co-precipitation approach was used to produce ZnS NPs from methanol plant extracts of *Tridax procumbens*, *Phyllanthusniruri*, and *Syzygium aromaticum* (Mani et al. 2018). In the presence of UV light, photocatalytic degradation of MB dye and MO dye by biosynthesized ZnS NPs in an aqueous medium was examined. The photocatalytic performance of synthesized ZnS NPs was enhanced because of the reduced particle size and lowered optical band gap. ZnS NPs were abbreviated as *Tridax-procumbens* plant extract synthesized ZnS — T: ZnS, *Phyllanthusniruri* plant extract synthesized ZnS — P:ZnS, and *Syzygium* aromaticum crude extract synthesized ZnS — S: ZnS (Mani et al. 2018).

The degradation of MB dye and MO dye in visible light irradiation was used to assess the photocatalytic performance of ZnS, T: ZnS, P: ZnS, and S: ZnS NPs samples. Before introducing the photocatalyst, MB dye and MO dye were subjected to a photocatalytic degradation process to determine concentration efficiency in visible light illumination. Consequently, both dyes degraded just 2% after 3 h of visible light irradiation. Furthermore, the same procedure was repeated with 1.0 mg of ZnS, T: ZnS, P: ZnS, and S: ZnS NPs. A promising photocatalyst acts to separate electron and hole pairs adequately. The holes of the VB interact with the MB dye and MO dye bounded surface, react with H_2O or OH^- and generate $^{\bullet}OH$ radicals. Then finally, the CB electron reduces the MB and MO dye's O_2 to $O_2^{\bullet-}$ to exert the degradation. After 3 hours of irradiation, the photocatalytic degradation efficiency of MB dye by using ZnS, T: ZnS, P: ZnS, and S: ZnS NPs as photocatalyst (1.0 mg) was reported to be 55%, 68%, 73% and 81% respectively, while that of MO dye under same conditions was 90%, 92%, 95% and 99% respectively (Mani et al. 2018).

Zn-based magnetic photocatalysts

Tetracycline (TC) is an antibiotic and it is used to cure common illnesses or protect against some forms of bacterial infections (Yu et al. 2019b). But it has environmental side effects and its residues are of great concern because they cause the extinction of essential species that are vital to the ecosystem. In addition, TC causes antibiotic resistance when used for extended periods (Reardon 2014; Ling et al. 2013; Chen and Liu 2016; Grenni et al. 2018). Yu et al. reported the photocatalytic degradation of TC using zinc-based magnetic photocatalyst (Yu et al. 2019b). ZnO, Ag_xO/ZnO, Fe_xO/ZnO, and Ag_xO/Fe_xO/ZnO are the photocatalysts investigated for the degradation of TC. The visible region ZnO absorption is greatly improved by doping ZnO with Ag. The charges produced on the ZnO under light are trapped by Ag, preventing charge recombination (Lai et al. 2010; Chen et al. 2011; Zhao et al. 2017; Yu et al. 2018). FeO_x extends the response of ZnO into the visible spectrum (Zhang et al. 2011; Wang et al. 2012a; Das et al. 2017). Pollutant degradation kinetics have been improved in ZnO doped with Ag- and Fe-ions (Yu et al. 2007, 2018; Lu et al. 2008; Wang et al. 2008, 2012a; Chu et al. 2010; Lai et al. 2010; Chen et al. 2011, 2015; Zhang et al. 2011; Amarjargal et al. 2013; Liu et al. 2015; Zhao et al. 2017; Das et al. 2017). Total organic carbon (TOC) was taken as a parameter for the extent of TC mineralization. Approximately 56.8% TOC was eliminated using Ag_xO(15%)/FeO_x(20%)/ZnO NTs. On the other hand, just 46.4, 49.3, and 50.2% of TOC were eliminated using bare ZnO, FeO_x(20%)/ZnO, and Ag_xO(15%)/ZnO, respectively (Yu et al. 2019b). The extent of TC-degradation in this report was higher as compared to any other earlier experimental study (Shirley 1972; Nogier and Delamar (1994); Briggs 2005). This method has advantages over other traditional methods as Ag_xO(15%)/FeO_x(20%)/ZnO nanotubes can be separated magnetically after the removal of TC. Consequently, the separation of photocatalysts becomes easy and less costly.

Cerium-based nanomaterials

Cerium oxide (CeO_2), ceria, is an n-type semiconductor with band gap energy (E_g) of about 3.19 eV (Elahi et al. 2019; Van Dao et al. 2019). In recent years, CeO_2 nanoparticles (CNPs) have drawn lots of attention due to their remarkable chemical and physical properties including excellent oxygen release/storage ability, high surface area, low dimensionality, low cost compared to the noble metal catalyst, strong absorption of the light in the UV region and chemical, and photo-corrosion resistance (Krishna Chandar and Jayavel 2014; Channei et al. 2014; Gnanam and Rajendran 2018; Van Dao et al. 2019). The catalytic performance of calcium-doped cerium oxide (CDC) was studied under various operating conditions such as irradiation period, initial MG concentration, photocatalyst dosage, and solution temperature. Furthermore, as the irradiation time was increased, the percentage degradation of MG increased slightly. The maximum value of percentage degradation (65.69%) was attained at 90 min irradiation time, after which, a slight decrease in the percentage degradation was observed (Amar et al. 2020).

Dyes have sparked a lot of attention due to their toxic effects, and effluents containing malachite green from dyeing, printing, and textile industries are left in nearby water streams, sometimes untreated or partially treated. Therefore, its degradation is necessary to make that water useful (Chawda et al. 2021). Moreover, as the MG initial concentration was increased above 6 mg/L, the percentage degradation decreased, reaching a lowest of 65.69% at an initial concentration of 10 mg/L. This could be because at high initial dye concentrations, dye molecules absorb more light than photocatalysts. As a result, the formation of $^{\bullet}OH$ and $^{\bullet}O_2^-$ radicals will be reduced, and photocatalyst activity will be decreased (Saleh and Djaja 2014). The impact of altering the photocatalyst (CDC) dosage from 0.04 to 0.14 g on the percentage dye degradation was examined. When the CDC amount was raised from 0.04 to 0.08 g, the percentage degradation of MG remained nearly constant (75%). Furthermore, as the CDC concentration was raised to 0.1 g, an increase in percentage degradation of up to 84.53% was reported. This could be due to the rise in the number of photocatalyst active sites, which increased the formation of $^{\bullet}OH$ radicals and, consequently, the percentage degradation of MG increased (Saleh and Djaja 2014; Sanna et al. 2016).

The study was carried out at three different solution temperatures (25, 35, and 45 °C), with a photocatalyst quantity of 0.1 g, a 90-min irradiation interval, and an initial MG concentration of 6 mg/L. When the solution temperature was raised from 25 °C (89.51%) to 35 °C, the percentage degradation slightly increased (92.52%). In addition, the percentage degradation of MG decreased slightly when the solution temperature was increased to 45 °C (90.86%) (Amar et al. 2020).

Whenever the CDC catalyst is exposed to UV light, holes in the VB are formed as the electrons in VB get stimulated and jump to the CB. These holes will interact with the surrounding H_2O to form extremely reactive hydroxyl radicals ($^{\bullet}OH$). In addition, when the produced electrons combine with the surrounding air O_2 molecules, extremely reactive oxygen radicals ($^{\bullet}O_2^-$) are produced (O_2) (see Eqs. 21–25). The photodegradation of MG is caused by this reactive species (Saikia et al. 2015; Murugan et al. 2018; Mandal et al. 2019; Amar et al. 2020).

$$Ca - CeO_2 + hv \rightarrow Ca - CeO_2 2(h^+ + e^-) \tag{21}$$

$$O_2 + e^- \rightarrow O_2{}^{\bullet -} \tag{22}$$

$$2e^- + O_2 + 2H^+ \rightarrow H_2O_2 \tag{23}$$

$$H_2O_2 + O_2{}^{\bullet -} \rightarrow HO^{\bullet} + OH^- \tag{24}$$

$$HO^{\bullet}/h^+/O_2{}^{\bullet -} + MG \rightarrow \text{Degraded product} \tag{25}$$

The cationic MG dye adsorption onto the TiO_2 surface proved challenging in acidic circumstances. The photocatalytic degradation of MG was slow because of the low concentration of the active $^{\bullet}OH$ radicals. The generation of active $^{\bullet}OH$ species is favored at higher pH levels, owing to enhanced hole transfer to adsorbed hydroxyls and electrostatic abstractive effects between operational cationic dyes and negatively charged TiO_2 particles. Even though MG dye can be adsorbed to some amount on the surface of TiO_2 in an alkaline medium. The MG dye molecules will transform to a leuco compound when the pH level has become too high ($pH = 11$) (Li et al. 1999).

Elahi et al. reported the fabrication of CeO_2 nanoparticles (CNPs) from the extract of Salvia Macrosiphon Boiss seeds and studied their photocatalytic capabilities for rhodamine B (RhB) dye degradation (Elahi et al. 2019). Results showed that lowering the particle size significantly increased the rate of the photocatalytic reaction, however, also increased the band gap energy contradictally.

The amount of catalyst is one of the most crucial factors that could influence the catalytic processes, hence varied concentrations of CNPs (50–250 mg) were utilized to assess its impact. It was observed that increasing the catalyst concentration up to 200 mg clearly increased the rate of RhB dye degradation, but after that point, there was no discernible change in the rate (Fig. 11a and b). The variation in RhB concentration after exposure durations with 200 mg of CNPs was shown in Fig. 11c. It was found that after 12 h of irradiation, the dye was almost

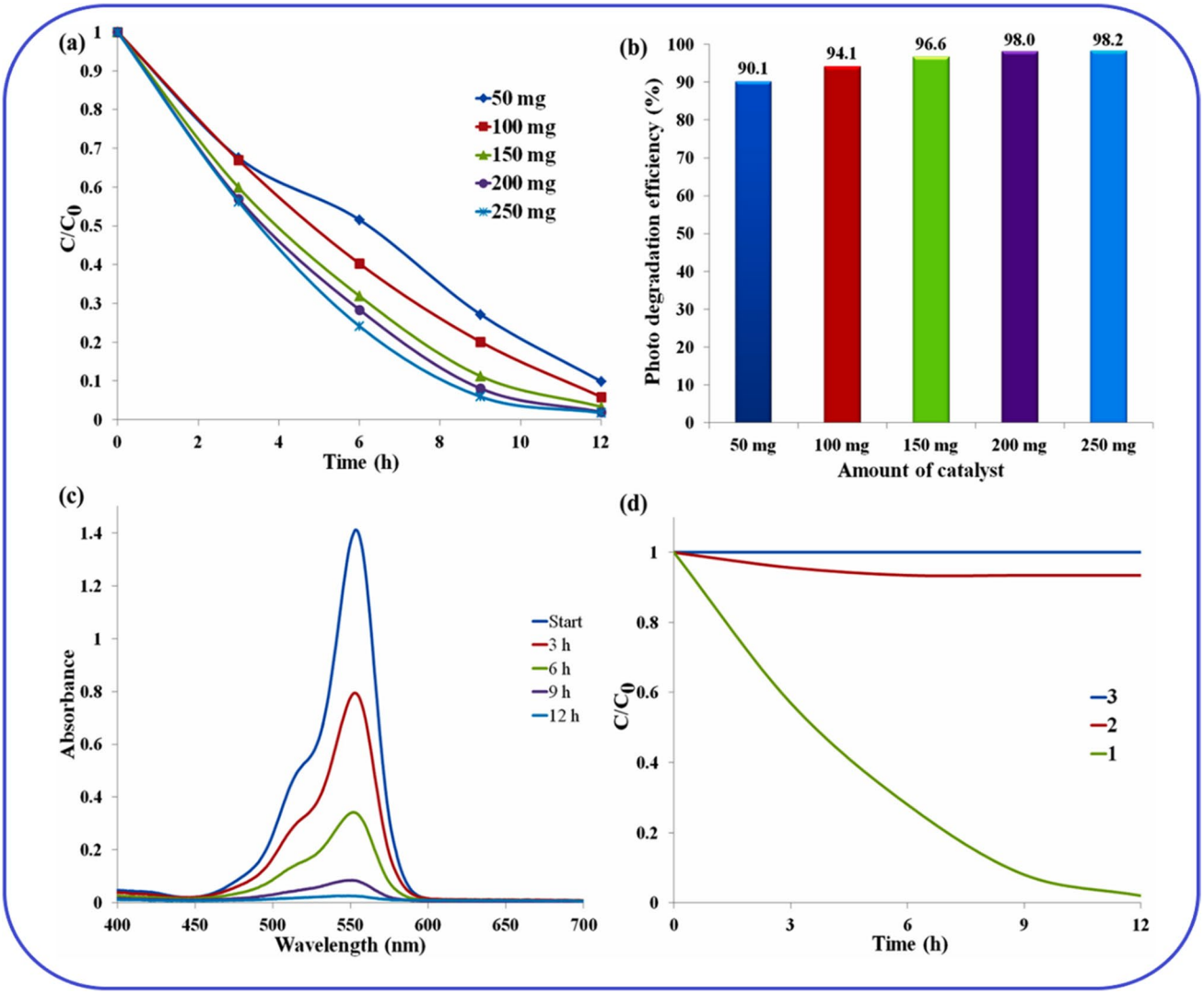

Fig. 11 **a** The photo-degradation rates of RhB dye for various CNPs-30 concentrations over time. **b** The photodegradation performances for various concentrations of CNP-30 following a 12-h exposure. **c** The visible spectra of RhB solution after exposure to UV-A light while containing 200 mg CNPs-30 during the course of time. **d** Correlation of the RhB photo-degradation efficiency of (1) 200 mg CNPs-30 when exposed to UV light for 30 min, (2) 200 mg CNPs-30 in dark, without even a catalyst over time. Reproduced with permission, copyright © 2020 Elsevier Ltd, (licence number — 5,347,491,038,761). All rights reserved (Elahi et al. 2019)

completely degraded. The degradation reaction was also carried out without the catalyst or in complete darkness (Fig. 11d), and the results demonstrated that the presence of CNPs and the exposure of the dye solution to UV light are essential for the efficient degradation of RhB.

Niobium-based photocatalysts

Using a hydrothermal process, Baeissa et al. reported the fabrication of sodium niobate ($NaNbO_3$) (Baeissa 2016). Then doping of sodium niobate nanocubes with gold was done. The findings showed that under visible light irradiation, Au/$NaNbO_3$ has greater efficiency for photocatalytic degradation of MG dye than sodium $NaNbO_3$ and TiO_2 Degussa.

Benzoquinone, tert-butanol, and sodium ethylenediaminetetraacetate (Na_2-EDTA) were examined for their effects as radical scavengers for superoxide anion radicals ($O_2\bullet-$), hydroxyl radicals ($^{\bullet}OH$), and holes, respectively. The observations showed that the amount of MG dye that was photocatalytically degraded was very small in the presence of 1 mM of Na_2-EDTA, indicating that photogenerated holes in the Au-$NaNbO_3$ are the principal reactive species that contributed to the degradation of MG dye. Additionally, the rate of photocatalytic degradation of MG dye gradually changed in the presence of benzoquinone. Therefore, in the photocatalytic degradation of MG dye, $O_2\bullet-$ and photogenerated holes are the primarily responsible species (Baeissa 2016). In the presence of three scavenger agents, Fig. 12 depicts

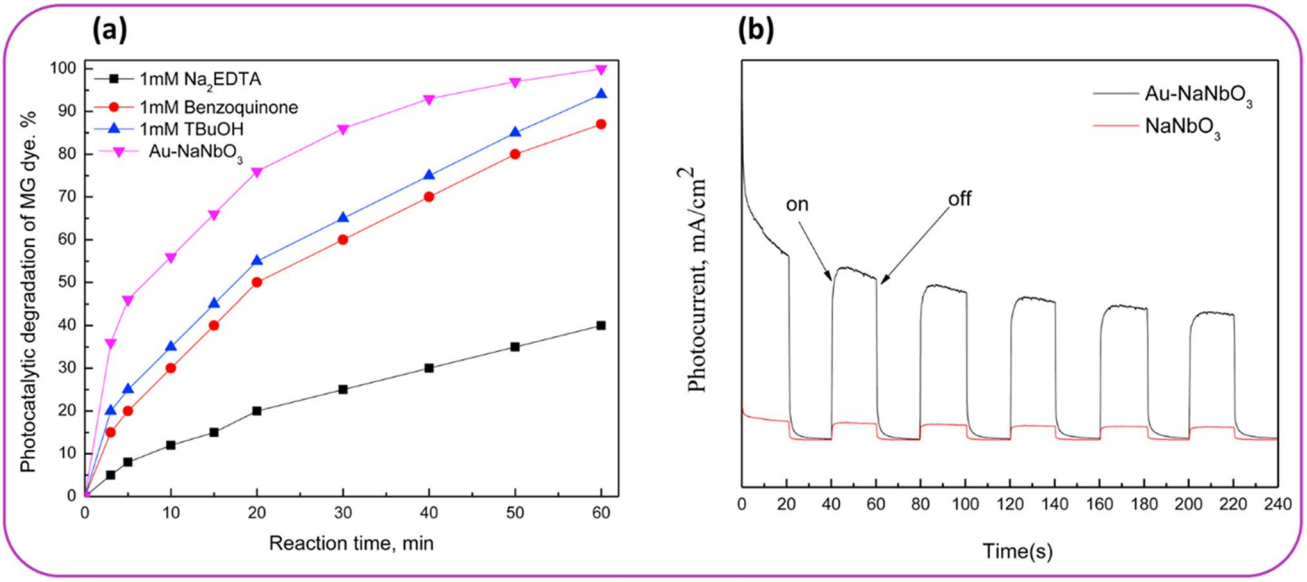

Fig. 12 **a** % Photocatalytic degradation of MG dye by Au-$NaNbO_3$ in the presence of three scavenger agents, **b** transient photocurrent responses of NaNbO3 and Au-$NaNbO_3$ photocatalyst. Reproduced with permission, copyright © 2020 Elsevier Ltd, (licence number — 5,347,491,505,417). All rights reserved (Baeissa 2016)

the photocatalytic degradation of MG dye, % Au-$NaNbO_3$, and Au-$NaNbO_3$.

This study showed that compared to $NaNbO_3$ photocatalyst, Au-$NaNbO_3$ photocatalyst has approximately nine times higher photocurrent density (Fig. 12b) (Baeissa 2016). Hence, Au-$NaNbO_3$ photocatalyst has high electron and hole pair separation efficiency and exhibited a low recombination rate.

Iron-based photocatalysts

Artificial food dyes are frequently employed in the food sector and contain organic groups such as amines, naphthalene, azo, sulfonate, phenolic, and thiol groups. These dyes can cause various issues, including eutrophication, bioaccumulation, water coloration, and odor (Barros et al. 2016). One of the most widely used food dyes is azorubine (AZB), which has been used largely in cheeses, cakes, candies, dried fruits, and several alcoholic beverages (Ahmadi et al. 2017; Kiayi et al. 2019). Traditional methods for the degradation of AZB have some disadvantages including the production of sludge (a process of coagulation), the requirement for regeneration (a process of adsorption), the production of concentrated effluent (a process of membrane), and the lack of mineralization (a process of coagulation and a process of adsorption) (Liu et al. 2021).

Bidgoli et al. demonstrated a novel approach for the degradation of AZB. AZB was degraded by a heterogeneous photo-assisted peroxymonosulfate (PMS) activation approach (Madihi-Bidgoli et al. 2021). Under the influence of UVA-LED radiation, Fe_2O_3, which was loaded onto a multi-wall carbon nanotube (Fe@MWCNT), was fabricated and used to activate PMS. Fe@MWCNT nano-catalyst for PMS activation performed better with higher Fe content *via* an electron transfer mechanism. Accordingly, for Fe:MWCNT ratios of 10%, 20%, 30%, and 40%, respectively, the AZB degradation efficiencies were 66.4%, 74.4%, 86.2%, and 82.5%. In an aqueous solution, the UVA-LED/Fe@MWCNT/PMS method removed approximately 95% of the AZB. After 6 cycles, it was noticed that the AZB removal rate dropped from 94.4 to 85.3%. This showed that Fe@MWCNT can be reused and is highly effective for PMS activation. Additionally, the amount of leached Fe was negligible (0.03–0.06 mg/L) throughout all cycles (Madihi-Bidgoli et al. 2021). These findings demonstrated that this catalyst has strong stability for repeated water usage without substantial leaching.

g-C_3N_4 and spinel-based photocatalysts

TiO_2 and ZnO are among the widely explored photocatalyst semiconductors. But large bandgap and nonmagnetic nature are the challenges with semiconductors. That is why semiconductors can only be used with UV radiation and are problematic to separate once the process of degradation is complete. However, this problem can be solved by utilizing a spinel catalyst, which has a narrow bandgap. Spinel ferrites are advantageous because they exhibit superior magnetic properties to semiconductors (Hanamura et al. 2003; Kirankumar and Sumathi 2020). Although

spinels are not as efficient as semiconductors even in UV light, combining both types of catalysts can be a promising way to overcome their respective shortcomings (Mamba and Mishra 2016). Composites made of semiconductors and spinel have the advantages of being easy to separate, utilizing nearly all of the UV and visible spectrum of sunlight, having a larger surface area, and numerous active sites (Parsons et al. 2009; Zhang et al. 2010; Govan and Gun'ko 2014; Gawande et al. 2015; Wang and Astruc 2017; Sun et al. 2019).

Acetaminophen (APAP), often known as paracetamol, is a common analgesic, antipyretic, and pain medication that is consumed in large quantities (1.45×10^5 tons/year) throughout the world (Noorisepehr et al. 2020). APAP is extremely resistant to conventional biological methods and is therefore difficult to degrade. Using a mesoporous composite ($CoFe_2O_4$/mpg-C_3N_4, CF/MCN) catalyst, Hassani et al. proposed a novel method for peroxymonosulfate (PMS) activation to decompose APAP (Hassani et al. 2020a). Under ideal pH, reaction time, and concentration of PMS and CF/MCN, more than 92% of APAP was degraded using CF/MCN/PMS. Less than 0.05 mg/L of Fe and Co leaching was observed, ensuring the stability of CF/MCN as a catalyst. Furthermore, leached metals had no impact on PMS activation and PMS activation-induced APAP degradation occurred heterogeneously (Hassani et al. 2020a). Pourshirband et al. reported the photodegradation of MO dye by CdS/g-C_3N_4 nanocatalyst (Pourshirband and Nezamzadeh-Ejhieh 2021). The designed catalyst can start the degradation of MO molecules through both oxidation and reduction routes. The photocatalyst's most significant reactive species in MO degradation are the photogenerated electron–hole pairs accumulated in the direct Z-scheme mechanism. In 90 min, more than 85% of MO molecules are broken down under optimized circumstances. There was no considerable loss in the photodegradation performance of CdS/g-C_3N_4 after 4 cycles under a pH of 3, which confirmed its high stability (Pourshirband and Nezamzadeh-Ejhieh 2021). MB dye can be degraded by sonocatalyst. One such sonocatalytic study was performed by Hassani et al. (2018). They fabricated cobalt ferrite/mesoporous graphitic carbon nitride ($CoFe_2O_4$/mpg-C_3N_4) nanocomposites and used it for MB dye degradation. It was observed that under optimal conditions of sonocatalysis, $CoFe_2O_4$/mpg-C_3N_4 degraded 92.81% of MB dye. This sonocatalyst was reusable because only a 9.6% reduction in its removal capability was noticed after 5 successive runs (Hassani et al. 2018). Shah et al. reported the fabrication of $NiFe_2O_4$ using the co-precipitation method (Shah et al. 2022). And further different amounts of TiO_2 were added to $NiFe_2O_4$ to make composites photocatalyst. Their photocatalytic performances were examined from the photocatalytic degradation of reactive turquoise blue 21 dye taken as model pollutants under the effect of solar light. The composite showed improved dye decolorization, mineralization, and efficient separation at the end of the process, as well as improved absorption of ultraviolet and visible light from the entire solar spectrum (Shah et al. 2022).

Jing et al. investigated the photocatalytic activities of composite Ag/Ag_3VO_4 and 5% $CoFe_2O_4$/ Ag/Ag_3VO_4 (Jing et al. 2016). These composites degraded 49.75 and 61.48% of tetracycline, correspondingly. This demonstrates that $CoFe_2O_4$ inclusion enhances activity, and even composites exhibit magnetic separability. The composites showed superior performance across a number of runs. Ye et al. studied the photocatalytic performance of core–shell organized $Fe_3O_4/SiO_2/TiO_2$ nanocomposites fabricated *via* the sol–gel method and compared it with that of SiO_2/TiO_2 (Ye et al. 2010b). Quick magnetic separation, high chemical stability, and preservation of the photocatalytic activity for at least 18 cycles are benefits of this composite. Like this, Wang et al. fabricated $Fe_3O_4/SiO_2/TiO_2$ nano-composites (NCs) *via* a sol–gel process and examined their photocatalytic activity on MB in an aqueous solution at $pH = 10$ at room temperature. The NCs demonstrated faster photodegradation of MB (78%) within 5 min of UV exposure (Wang et al. 2012b) (Table 3).

Challenges

The surface of the material, photo-generation of electrons and hole, and band gap are the factors that influence the photocatalytic activity of the material. Photocatalysts with an extensive range of photo absorption and higher separation efficiency of photo-induced charge carriers are required for photocatalytic activity. However, most current photocatalytic materials have a poor solar radiation utilization efficiency and a high photogenerated charge carrier recombination rate, which restricts overall quantum efficiency and practical applications. Some nanomaterials photocatalysts such as TiO_2 exhibit various limitations and have many challenges that rigorously restrict their feasible applications and efficiencies. The nanomaterials metal sulfides photocatalysts also face various obstacles, the most prevalent of which are the mode of fabrication, use of toxic solvents, etc. These challenges restrict the use of nanomaterials metal sulfides photocatalysts in several applications. Furthermore, the efficiencies of these nanomaterials metal sulfides photocatalysts are also affected by other factors such as the photo-generation of the electron–hole pair, band gap, and the surface of the material of nanostructures. The photocatalytic dye degradation also depends upon the wastewater matrix. The removal efficiency in highly charged water is significantly impacted by dissolved and suspended components. However, dissolved substances may have positive, negative, or neutral effects and may influence the photocatalytic water disinfection procedure. Scavengers could also inhibit the removal of

Table 3 Details of various photocatalysts with their degradation efficiencies for different dyes

Sr. no	Photocatalyst	Method of synthesis	Morphology	Light source	Photocatalytic performance	Applications	Ref
1	Titanium dioxide	Electrochemical anodization	Nanotubes	UVA irradiation	The specific reaction rate for IC dye is 74.14% and RB5 dye is 65.71%	Decolorization of Indigo Carmine and Reactive Black 5	(Rojviroon et al. 2021)
2	Titanium dioxide	Template synthesis	Hollow nanofibres	30 W UV lamp with $\lambda = 312$ nm	Efficiency = 85%	Photocatalytic oxidation of MB dye	(Jafri et al. 2021)
3	Cadmium Sulfide	Using the extract of Dicliptera Roxburghiana	Spherical	Solar light irradiation	Efficiency = 87.12%	Photocatalytic degradation of MB dye	(Ullah et al. 2021)
4	Calcium molybdate (undoped and C-doped)	Hydrothermal method	Spherical	200 W Tungsten lamp	K (2% C-doped) = 11.60×10^5 at 5×10^4 mol/L dye concentration	Photocatalytic oxidation of malachite green	(Chawda et al. 2021)
5	Zinc oxide	Using Alchemilla Vulgaris leaves	Cauliflower shape	500 W Xenon lamp	Efficiency = 75%	Photocatalytic degradation of rhodamine B (RhB) dye	(Rajendrachari et al. 2021)
6	TiO_2 (pure and Sn & F doped)	Solid-state reaction	Spherical and ellipsoid	Visible light irradiation	MB degradation efficiency of TiO_2 and TSF20 = 60% and 86%. MO degradation efficiency of TO_2 and TSF20 = 65% and 77%	Photocatalytic degradation of MB and MO dye	Ancy et al. 2021)
7	Mg-Zn ferrite	Combustion method	Spherical	UV lamp irradiation	K(MZF1) = 0.011/min and K(MZF3) = 0.002/min	Photocatalytic reduction of MB dye	(Bessy et al. 2022)
8	Ag-TiO_2/Perlite	Sol–gel	Highly porous structure with a rough surface	Solar light irradiation	Efficiency = 95.54%	Photocatalytic degradation of MB dye	(Pham Xuan et al. 2020)
9	CuO-VO_2/TiO_2	Hydrothermal method	Nanotubes/ Nanosheets	500 W Tungsten lamp	Rate constant for MB, MO, and congo red (CR) dyes = 0.34, 0.090, and 0.155 min^{-1}, respectively	Photocatalytic oxidation of MB, MO and CR dye	(Shammi et al. 2021)
10	$CoFe_2O_4 - gC_3N_4$	Thermal treatment followed by ultrasonication	Spherical	150 W Xenon lamp	Efficiency (50 CF − 50 g C_3N_4) ~ 100% for MB degradation in 45 min ~100% for MO degradation in 1.5 h ~100% for CR degradation in 1.5 h	Photodegradation of MB, MO, CR, Turq CL-B, Yell CL-2R, and Red CL-5B	(Gogoi et al. 2021)

Table 3 (continued)

Sr. no	Photocatalyst	Method of synthesis	Morphology	Light source	Photocatalytic performance	Applications	Ref
11	Silver nanoparticles	Green synthesis using the fruit extract of Terminalia bellirica		Solar irradiation		Photocatalytic degradation of MB dye	(Sharma 2021)

dissolved organic materials if they are present in the water matrix (DOM). Natural organic materials, carbonates, bromides, and bicarbonate types, for instance, can act as •OH scavengers in neutral water. Additionally, as water matrix complexity grows, the efficiency to remove contaminants decreases. It is because of competition between organic and inorganic components for the catalytic active sites. Light absorption and light mitigation are additional major hindrances in the water matrix. As a result, the cohabitation of organic and inorganic materials in a complex water matrix leads to a harmful impact during photocatalytic treatment. Inorganic salts like NaCl, $FeCl_2$, $CaCl_2$ $FeCl_3$, and $AlCl_3$ that are present in the water matrix have a detrimental influence on photocatalytic reactions and can even totally stop these reactions when they are present in large concentrations in the wastewater.

Conclusion: future perspective

The rising demand for clean water and a scarcity of it due to fast urbanism, rise in population, and climate change has become unprecedented worldwide challenges. Water purification is a top priority for human usage, industry, ecosystem management, and agriculture around the world. The use of nanoparticles in water sanitization is quite effective. The significant water-polluting species are toxic heavy metal ions and various organic dyes. The traditional techniques for reducing these heavy metal ions and degradation of organic dyes have many drawbacks, including excessive sludge formation, high energy consumption, low removal efficiency and expensive removal, and generation of secondary pollutants. As a result, researchers have been making great efforts to design eco-friendly, energy-efficient, and low-cost water treatment techniques to improve water purification. Photocatalysts are a significantly emerging species with great potential to reduce heavy metal ions and degrade organic dyes. Photocatalysis has various advantages over traditional methods for wastewater treatment as photocatalysts have higher catalytic efficiencies, take a small interval for the reactions, and do not form secondary hazardous products. In the present review, numerous photocatalysts for photodegradation of various dyes in wastewater for environmentally-friendly purposes and to reduce various heavy metal ions are well described. Among various photocatalysts, nano-photocatalysts are more efficient in wastewater treatment because they have been shown to have greater photocatalytic efficiencies for dye degradation. In addition, magnetic photocatalysts are advantageous because their separation after the degradation of dye is highly cost-effective. Semiconductor and spinel composites have the benefits of being easy to separate, absorbing the entire UV and visible spectrum of sunlight practically, having a greater surface area, and

having numerous active sites. The mechanism proposed for various photocatalysts has also been detailed. The doped photocatalysts and those synthesized via green methods, i.e., photocatalysts made of metal sulfides nanostructures, have shown to have the potential for improved photocatalytic degradation of various dyes. The fabrication of metal sulfide nanostructures using plants, bacteria, and fungi is straightforward and environmentally beneficial.

Author contribution All authors contributed to the review study by writing and editing. The first draft writing, data collection, and analysis were performed equally by Permender Singh and Brij Mohan. Comments on previous versions of the manuscript by Vasundhara Madaan, Rohit Ranga, Parveen Kumari, Sandeep Kumar, Vinita Bhankar, and Parmod Kumar. Conceptualization, investigation, and resources by Krishan Kumar. All authors read and approved the final manuscript.

Funding Permender Singh is grateful for financial support to the Council of Scientific and Industrial Research (CSIR), New Delhi, India, through Junior Research Fellowship (JRF) (Award letter No. 09/1063(0035)2021-EMR-I, 14/01/2021.

Data availability Since our paper is a review, all the data/information/figure analyzed has been cited separately, and no data has been generated.

Declarations

Ethics approval and consent to participate Not applicable.

Consent for publication Not applicable.

Competing interests The authors declare no competing interests.

References

Agustina TE, Ang HM, Vareek VK (2005) A review of synergistic effect of photocatalysis and ozonation on wastewater treatment. J Photochem Photobiol C Photochem Rev 6:264–273. https://doi.org/10.1016/J.JPHOTOCHEMREV.2005.12.003

Ahmad S, Aadil M, Ejaz SR et al (2022) Sol-gel synthesis of nanostructured ZnO/$SrZnO_2$ with boosted antibacterial and photocatalytic activity. Ceram Int 48:2394–2405. https://doi.org/10.1016/j.ceramint.2021.10.020

Ahmadi M, Ghanbari F, Alvarez A, Silva Martinez S (2017) UV-LEDs assisted peroxymonosulfate/Fe^{2+} for oxidative removal of carmoisine: the effect of chloride ion. Korean J Chem Eng 34:2154–2161. https://doi.org/10.1007/s11814-017-0122-1

Akpan UG, Hameed BH (2009) Parameters affecting the photocatalytic degradation of dyes using TiO_2-based photocatalysts: a review. J Hazard Mater 170:520–529. https://doi.org/10.1016/J.JHAZMAT.2009.05.039

Al-Mamun MR, Kader S, Islam MS, Khan MZH (2019) Photocatalytic activity improvement and application of UV-TiO_2 photocatalysis in textile wastewater treatment: a review. J Environ Chem Eng 7. https://doi.org/10.1016/j.jece.2019.103248

Albergamo V, Escher BI, Schymanski EL et al (2020) Evaluation of reverse osmosis drinking water treatment of riverbank filtrate using bioanalytical tools and non-target screening. Environ Sci Water Res Technol 6:103–116. https://doi.org/10.1039/c9ew00741e

Alhakimi G, Studnicki LH, Al-Ghazali M (2003) Photocatalytic destruction of potassium hydrogen phthalate using TiO_2 and sunlight: application for the treatment of industrial wastewater. Elsevier. J Photochem Photobiol A: Chem 154:219–228. https://doi.org/10.1016/S1010-6030(02)00329-5

Alidokht L, Hassani A, Karaca S, Khataee A (2013) Response surface analysis of removal of a textile dye by a Turkish coal powder A Chemiluminescent Method for the Detection of H_2O_2 and Glucose Based on Intrinsic Peroxidase-Like Activity of WS_2 Quantum Dots View project Dry reforming of methane over promo. Adv Environ Res 2:291–308. https://doi.org/10.12989/aer.2013.2.4.291

Amanulla M, Magdalane CM, Ramalingam G et al (2022) Fabrication and characterization of $Th(MoO_4)_2/TiO_2$ nanocomposite for potential use in photocatalytic degradation of toxic pollutants. Appl Phys A 128(5):1–21. https://doi.org/10.1007/S00339-022-05504-1

Amar IA, Harara HM, Baqul QA et al (2020) Photocatalytic degradation of malachite green dye under UV light irradiation using calcium-doped ceria nanoparticles. Asian J Nanosci Mater 3:1–14. https://doi.org/10.26655/AJNANOMAT.2020.1.1

Amarjargal A, Tijing LD, Im IT, Kim CS (2013) Simultaneous preparation of Ag/Fe_3O_4 core-shell nanocomposites with enhanced magnetic moment and strong antibacterial and catalytic properties. Chem Eng J 226:243–254. https://doi.org/10.1016/j.cej.2013.04.054

An S, Joshi BN, Lee MW et al (2014) Electrospun graphene-ZnO nanofiber mats for photocatalysis applications. Appl Surf Sci 294:24–28. https://doi.org/10.1016/j.apsusc.2013.12.159

Ancy K, Vijilvani C, Bindhu MR et al (2021) Visible light assisted photocatalytic degradation of commercial dyes and waste water by Sn-F co-doped titanium dioxide nanoparticles with potential antimicrobial application. Chemosphere 277. https://doi.org/10.1016/J.CHEMOSPHERE.2021.130247

Anwer H, Mahmood A, Lee J et al (2019) Photocatalysts for degradation of dyes in industrial effluents: opportunities and challenges. Nano Res 12:955–972. https://doi.org/10.1007/s12274-019-2287-0

Ayati A, Tanhaei B, Bamoharram FF et al (2016) Photocatalytic degradation of nitrobenzene by gold nanoparticles decorated polyoxometalate immobilized TiO_2 nanotubes. Sep Purif Technol 171:62–68. https://doi.org/10.1016/j.seppur.2016.07.015

Ayodhya D, Veerabhadram G (2017) One-pot green synthesis, characterization, photocatalytic, sensing and antimicrobial studies of Calotropis gigantea leaf extract capped CdS NPs. Mater Sci Eng B 225:33–44. https://doi.org/10.1016/J.MSEB.2017.08.008

Babu DS, Srivastava V, Nidheesh PV, Kumar MS (2019) Detoxification of water and wastewater by advanced oxidation processes. Sci Total Environ 696:133961. https://doi.org/10.1016/j.scitotenv.2019.133961

Baeissa ES (2016) Photocatalytic degradation of malachite green dye using Au/$NaNbO_3$nanoparticles. J Alloys Compd 672:564–570. https://doi.org/10.1016/j.jallcom.2016.02.024

Bagheri M, Najafabadi NR, Borna E (2020) Removal of reactive blue 203 dye photocatalytic using ZnO nanoparticles stabilized on functionalized MWCNTs. J King Saud Univ - Sci 32:799–804. https://doi.org/10.1016/j.jksus.2019.02.012

Bahnemann D (2004) Photocatalytic water treatment: solar energy applications. Sol Energy 77:445–459. https://doi.org/10.1016/J.SOLENER.2004.03.031

Balcioğlu IA, Inel Y (1996) Photocatalytic degradation of organic contaminants in semiconductor suspensions with added H_2O_2. J Environ Sci Heal - Part A Toxic/hazardous Subst Environ Eng 31:123–138. https://doi.org/10.1080/10934529609376347

Baron J (2008) Issues in ecology. Bull Ecol Soc Am 89:341–343. https://doi.org/10.1890/0012-9623(2008)89[341:iie]2.0.co;2

Barros WRP, Steter JR, Lanza MRV, Tavares AC (2016) Catalytic activity of $Fe_{3-x}Cu_xO_4$ ($0 \leq x \leq 0.25$) nanoparticles for the degradation of Amaranth food dye by heterogeneous electro-Fenton process. Appl Catal B Environ 180:434–441. https://doi.org/10.1016/j.apcatb.2015.06.048

Bessy TC, Bindhu MR, Johnson J, et al (2022) UV light assisted photocatalytic degradation of textile waste water by $Mg_{0.8-x}Zn_xFe_2O_4$ synthesized by combustion method and in-vitro antimicrobial activities. Environ Res 204. https://doi.org/10.1016/J.ENVRES.2021.111917

Bolto B, Dixon D, Eldridge R et al (2002) Removal of natural organic matter by ion exchange. Water Res 36:5057–5065. https://doi.org/10.1016/S0043-1354(02)00231-2

Bonnefond A, González E, Asua JM et al (2015) New evidence for hybrid acrylic/TiO_2 films inducing bacterial inactivation under low intensity simulated sunlight. Colloids Surfaces B Biointerfaces 135:1–7. https://doi.org/10.1016/j.colsurfb.2015.07.034

Boroski M, Rodrigues AC, Garcia JC et al (2009) Combined electrocoagulation and TiO_2 photoassisted treatment applied to wastewater effluents from pharmaceutical and cosmetic industries. J Hazard Mater 162:448–454. https://doi.org/10.1016/j.jhazmat.2008.05.062

Braun AM (2003) Photochemical purification of water and air. By Thomas Oppenländer. Angew Chemie Int Ed 42:5117–5117. https://doi.org/10.1002/anie.200385988

Briggs D (2005) X-ray photoelectron spectroscopy (XPS). Handb Adhes Second Ed 621–622. https://doi.org/10.1002/0470014229.ch22

Brillas E (2020) A review on the photoelectro-Fenton process as efficient electrochemical advanced oxidation for wastewater remediation. Treatment with UV light, sunlight, and coupling with conventional and other photo-assisted advanced technologies. Chemosphere 250:126198. https://doi.org/10.1016/j.chemosphere.2020.126198

Butler EC, Davis AP (1993) Photocatalytic oxidation in aqueous titanium dioxide suspensions: the influence of dissolved transition metals. J Photochem Photobiol A Chem 70:273–283. https://doi.org/10.1016/1010-6030(93)85053-B

Campinas M, Viegas RMC, Coelho R et al (2021) Adsorption/coagulation/ceramic microfiltration for treating challenging waters for drinking water production. Membranes (basel) 11:1–19. https://doi.org/10.3390/membranes11020091

Carolin CF, Kumar PS, Saravanan A et al (2017) Efficient techniques for the removal of toxic heavy metals from aquatic environment: a review. J Environ Chem Eng 5:2782–2799. https://doi.org/10.1016/j.jece.2017.05.029

Castro-Muñoz R, González-Melgoza LL, García-Depraect O (2021) Ongoing progress on novel nanocomposite membranes for the separation of heavy metals from contaminated water. Chemosphere 270. https://doi.org/10.1016/j.chemosphere.2020.129421

Cattarin S, Decker F (2009) Electrodes | semiconductor electrodes. Encycl Electrochem Power Sources 9:121–133. https://doi.org/10.1016/B978-044452745-5.00031-9

Channei D, Inceesungvorn B, Wetchakun N et al (2014) Photocatalytic degradation of methyl orange by CeO_2 and Fe–doped CeO_2 films under visible light irradiation. Sci Reports 41(4):1–7. https://doi.org/10.1038/srep05757

Chauhan PS, Kant R, Rai A et al (2019) Facile synthesis of ZnO/GO nanoflowers over Si substrate for improved photocatalytic decolorization of MB dye and industrial wastewater under solar irradiation. Mater Sci Semicond Process 89:6–17. https://doi.org/10.1016/J.MSSP.2018.08.022

Chawda HS, Bhatt J, Rathore R, Ameta SC, Ameta R (2021) Photocatalytic degradation of malachite green using undoped and carbon-doped calcium molybdate catalysts. J Adv Chem Sci 7:725–728. https://doi.org/10.30799/JACS.237.21070202

Chen CC, Lu CS, Chung YC, Jan JL (2007) UV light induced photodegradation of malachite green on TiO_2 nanoparticles. J Hazard Mater 141:520–528. https://doi.org/10.1016/J.JHAZMAT.2006.07.011

Chen D, Huang F, Ren G et al (2010) ZnS nano-architectures: photocatalysis, deactivation and regeneration. Nanoscale 2:2062–2064. https://doi.org/10.1039/C0NR00171F

Chen J, Hu B, Zhi J (2016a) Optical and photocatalytic properties of Corymbia citriodora leaf extract synthesized ZnS nanoparticles. Phys E Low-Dimens Syst Nanostruct 79:103–106. https://doi.org/10.1016/J.PHYSE.2015.12.015

Chen R, Zou C, Bian J, et al (2011) Microstructure and optical properties of Ag-doped ZnO nanostructures prepared by a wet oxidation doping process. Nanotechnology 22. https://doi.org/10.1088/0957-4484/22/10/105706

Chen S, Yan R, Zhang X et al (2017) Photogenerated electron modulation to dominantly induce efficient 2,4-dichlorophenol degradation on BiOBr nanoplates with different phosphate modification. Appl Catal B Environ 209:320–328. https://doi.org/10.1016/j.apcatb.2017.03.003

Chen X, Di L, Yang H, Xian T (2019) A magnetically recoverable $CaTiO_3$/reduced graphene oxide/$NiFe_2O_4$ nanocomposite for the dye degradation under simulated sunlight irradiation. J Ceram Soc Japan 127:221–231. https://doi.org/10.2109/jcersj2.18168

Chen Y, Liu K (2016) Preparation and characterization of nitrogen-doped TiO_2/diatomite integrated photocatalytic pellet for the adsorption-degradation of tetracycline hydrochloride using visible light. Chem Eng J 302:682–696. https://doi.org/10.1016/j.cej.2016.05.108

Chen Y, Ma Q, Jia H, Wang Y (2016b) Hydrothermal synthesis of ZnS microspheres with highly effective photocatalytic and antibacterial properties. J Mater Sci Mater Electron 27:10237–10243. https://doi.org/10.1007/S10854-016-5102-4

Chen Y, Zhao H, Liu B, Yang H (2015) Charge separation between wurtzite ZnO polar 001 surfaces and their enhanced photocatalytic activity. Appl Catal B Environ 163:189–197. https://doi.org/10.1016/j.apcatb.2014.07.044

Cheng M, Ma W, Li J et al (2004) Visible-light-assisted degradation of dye pollutants over Fe(III)-loaded resin in the presence of H_2O_2 at neutral pH values. Environ Sci Technol 38:1569–1575. https://doi.org/10.1021/ES034442X

Chenthamarakshan CR, Rajeshwar K, Wolfrum EJ (2000) Heterogeneous photocatalytic reduction of Cr(VI) in UV-irradiated titania suspensions: effect of protons, ammonium ions, and other interfacial aspects. Langmuir 16:2715–2721. https://doi.org/10.1021/la9911483

Choi W, Termin A, Hoffmann MR (1994) The role of metal ion dopants in quantum-sized TiO_2: correlation between photoreactivity and charge carrier recombination dynamics. J Phys Chem 98:13669–13679. https://doi.org/10.1021/j100102a038

Chu D, Masuda Y, Ohji T, Kato K (2010) Formation and photocatalytic application of ZnO nanotubes using aqueous solution. Langmuir 26:2811–2815. https://doi.org/10.1021/la902866a

Colmenares JC, Luque R, Campelo JM et al (2009) Nanostructured photocatalysts and their applications in the photocatalytic transformation of lignocellulosic biomass: an overview. Materials (basel) 2:2228–2258. https://doi.org/10.3390/ma2042228

Dabirvaziri B, Givianrad MH, Sourinejad I, Moradi AM, Mostafavi PG et al (2019) A simple and effective synthesis of magnetic γ-Fe_2O_3@SiO_2@TiO_2 – Ag microspheres as a recyclable photocatalyst : dye degradation and antibacterial potential. J Environ Health Sci Eng 17:949–960 https://doi.org/10.1007/s40201-019-00410-w

Das S, Narayanam C, Roy S, Khanna R (2017) A model of wetting of partially wettable porous solids by thin liquid films. Chem Eng J 320:104–115. https://doi.org/10.1016/j.cej.2017.02.151

Dimitroula H, Daskalaki VM, Frontistis Z et al (2012) Solar photocatalysis for the abatement of emerging micro-contaminants in wastewater: synthesis, characterization and testing of various TiO_2 samples. Appl Catal B Environ 117–118:283–291. https://doi.org/10.1016/j.apcatb.2012.01.024

Eghbali P, Hassani A, Sündü B, Metin Ö (2019) Strontium titanate nanocubes assembled on mesoporous graphitic carbon nitride ($SrTiO_3$/mpg-C_3N_4): preparation, characterization and catalytic performance. J Mol Liq 290:111208. https://doi.org/10.1016/j.molliq.2019.111208

Einert M, Hartmann P, Smarsly B, Brezesinski T (2021) Quasi-homogenous photocatalysis of quantum-sized Fe-doped TiO_2 in optically transparent aqueous dispersions. Sci Reports 111(11):1–10. https://doi.org/10.1038/s41598-021-96911-6

Ekka B, Sahu MK, Patel RK, Dash P (2019) Titania coated silica nanocomposite prepared via encapsulation method for the degradation of Safranin-O dye from aqueous solution: optimization using statistical design. Water Resour Ind 22. https://doi.org/10.1016/j.wri.2016.08.001

Elahi B, Mirzaee M, Darroudi M et al (2019) Preparation of cerium oxide nanoparticles in Salvia Macrosiphon Boiss seeds extract and investigation of their photo-catalytic activities. Ceram Int 45:4790–4797. https://doi.org/10.1016/J.CERAMINT.2018.11.173

Erfani M, Javanbakht V (2018) Methylene blue removal from aqueous solution by a biocomposite synthesized from sodium alginate and wastes of oil extraction from almond peanut. Int J Biol Macromol 114:244–255. https://doi.org/10.1016/j.ijbiomac.2018.03.003

Esania Z, Younesi H, Nowrouzi M, Karimi-Maleh H (2022) Characterization and assessment of the photocatalytic activity of ZnO-Fe_3O_4/TiO_2 nanocomposite based on MIL-125(Ti) synthesized by mixed solvo-hydrothermal and sol-gel methods. J Water Process Eng 47:102750. https://doi.org/10.1016/j.jwpe.2022.102750

Fang Z, Gao Y, Bolan N et al (2020) Conversion of biological solid waste to graphene-containing biochar for water remediation: a critical review. Chem Eng J 390:124611. https://doi.org/10.1016/j.cej.2020.124611

Fatima B, Siddiqui SI, Ahmed R, Chaudhry SA (2019) Green synthesis of f-$CdWO_4$ for photocatalytic degradation and adsorptive removal of Bismarck Brown R dye from water. Water Resour Ind 22:100119. https://doi.org/10.1016/j.wri.2019.100119

Fujishima A, Rao TN, Tryk DA et al (2000) Titanium dioxide photocatalysis. J Photochem Photobiol C: Photochem Rev 1:1–21. https://doi.org/10.1016/S1389-5567(00)00002-2

Gao X, Kong C-P, Jia R et al (2018) Influence of one-dimensional TiO_2 nanotube on interfacial electron transfer in dye-sensitized solar cells: insights from theoretical investigation. Sol Energy 176:545–555. https://doi.org/10.1016/j.solener.2018.10.061

García-Fernández I, Fernández-Calderero I, Inmaculada Polo-López M, Fernández-Ibáñez P (2015) Disinfection of urban effluents using solar TiO_2 photocatalysis: a study of significance of dissolved oxygen, temperature, type of microorganism and water matrix. Catal Today 240:30–38. https://doi.org/10.1016/j.cattod.2014.03.026

García-Fernández I, Miralles-Cuevas S, Oller I et al (2019) Inactivation of E. coli and E. faecalis by solar photo-Fenton with EDDS complex at neutral pH in municipal wastewater effluents. J Hazard Mater 372:85–93. https://doi.org/10.1016/j.jhazmat.2018.07.037

Gawande MB, Monga Y, Zboril R, Sharma RK (2015) Silica-decorated magnetic nanocomposites for catalytic applications. Coord Chem Rev 288:118–143. https://doi.org/10.1016/j.ccr.2015.01.001

Ghanbari F, Giannakis S, Lin KYA et al (2021) Acetaminophen degradation by a synergistic peracetic acid/UVC-LED/Fe(II) advanced oxidation process: kinetic assessment, process feasibility and mechanistic considerations. Chemosphere 263:128119. https://doi.org/10.1016/j.chemosphere.2020.128119

Ghanbari F, Moradi M (2017) Application of peroxymonosulfate and its activation methods for degradation of environmental organic pollutants: review. Chem Eng J 310:41–62. https://doi.org/10.1016/j.cej.2016.10.064

Ghanbari F, Zirrahi F, Olfati D et al (2020) TiO_2 nanoparticles removal by electrocoagulation using iron electrodes: catalytic activity of electrochemical sludge for the degradation of emerging pollutant. J Mol Liq 310:113217. https://doi.org/10.1016/j.molliq.2020.113217

Giannakas AE, Seristatidou E, Deligiannakis Y, Konstantinou I (2013) Photocatalytic activity of N-doped and N-F co-doped TiO_2 and reduction of chromium(VI) in aqueous solution: An EPR study. Appl Catal B Environ 132–133:460–468. https://doi.org/10.1016/j.apcatb.2012.12.017

Giannakis S, Rtimi S, Pulgarin C (2017) Light-assisted advanced oxidation processes for the elimination of chemical and microbiological pollution of wastewaters in developed and developing countries. Molecules 22. https://doi.org/10.3390/molecules22071070

Giménez J, Aguado MA, Cervera-March S (1996) Photocatalytic reduction of chromium(VI) with titania powders in a flow system. Kinetics and catalyst activity. J Mol Catal A Chem 105:67–78. https://doi.org/10.1016/1381-1169(95)00148-4

Gnanam S, Rajendran V (2018) Facile sol-gel preparation of Cd-doped cerium oxide (CeO_2) nanoparticles and their photocatalytic activities. J Alloys Compd 735:1854–1862. https://doi.org/10.1016/J.JALLCOM.2017.11.330

Gnaser H, Savina MR, Calaway WF et al (2005) Photocatalytic degradation of methylene blue on nanocrystalline TiO_2: surface mass spectrometry of reaction intermediates. Int J Mass Spectrom 245:61–67. https://doi.org/10.1016/j.ijms.2005.07.003

Gogoi D, Makkar P, Ghosh NN (2021) Solar light-irradiated photocatalytic degradation of model dyes and industrial dyes by a magnetic $CoFe_2O_4$-gC_3N_4 S-scheme heterojunction photocatalyst. ACS Omega 6:4831–4841. https://doi.org/10.1021/ACSOMEGA.0C05809

Görgün N, Özer Ç, Polat K (2019) A new catalyst material from electrospun PVDF-HFP nanofibers by using magnetron-sputter coating for the treatment of dye-polluted waters. Adv Compos Hybrid Mater 2:423–430. https://doi.org/10.1007/s42114-019-00105-8

Govan J, Gun'ko YK (2014) Recent advances in the application of magnetic nanoparticles as a support for homogeneous catalysts. Nanomaterials 4:222–241. https://doi.org/10.3390/nano4020222

Grao M, Ratova M, Amorim CC et al (2020) Crystalline TiO_2 supported on stainless steel mesh deposited in a one step process via pulsed DC magnetron sputtering for wastewater treatment applications. J Mater Res Technol 9:5761–5773. https://doi.org/10.1016/j.jmrt.2020.03.101

Grenni P, Ancona V, Barra Caracciolo A (2018) Ecological effects of antibiotics on natural ecosystems: a review. Microchem J 136:25–39. https://doi.org/10.1016/j.microc.2017.02.006

Gunarathne V, Rajapaksha AU, Vithanage M, et al (2020) Hydrometallurgical processes for heavy metals recovery from industrial sludges. 101080/1064338920201847949. https://doi.org/10.1080/10643389.2020.1847949

Hanamura E, Kawabe Y, Takashima H et al (2003) Optical properties of transition-metal doped spinels. J Nonlinear Opt Phys Mater 12:467–473. https://doi.org/10.1142/S0218863503001584

Hariharan C (2006) Photocatalytic degradation of organic contaminants in water by ZnO nanoparticles: revisited. Appl Catal A Gen 304:55–61. https://doi.org/10.1016/J.APCATA.2006.02.020

Harish R, Samuel J, Mishra R et al (2012) Bio-reduction of Cr(VI) by exopolysaccharides (EPS) from indigenous bacterial species

of Sukinda chromite mine, India. Biodegradation 23:487–496. https://doi.org/10.1007/S10532-011-9527-4

Hassani A, Eghbali P, Kakavandi B et al (2020a) Acetaminophen removal from aqueous solutions through peroxymonosulfate activation by $CoFe_2O_4$/mpg-C_3N_4 nanocomposite: insight into the performance and degradation kinetics. Environ Technol Innov 20:101127. https://doi.org/10.1016/j.eti.2020.101127

Hassani A, Eghbali P, Metin Ö (2018) Sonocatalytic removal of methylene blue from water solution by cobalt ferrite/mesoporous graphitic carbon nitride ($CoFe_2O_4$/mpg-C_3N_4) nanocomposites: response surface methodology approach. Environ Sci Pollut Res 25:32140–32155. https://doi.org/10.1007/s11356-018-3151-3

Hassani A, Faraji M, Eghbali P (2020b) Facile fabrication of mpg-C_3N_4/Ag/ZnO nanowires/Zn photocatalyst plates for photodegradation of dye pollutant. J Photochem Photobiol A Chem 400:112665. https://doi.org/10.1016/j.jphotochem.2020.112665

Hosseini-Zori M (2018) Co-doped TiO_2 nanostructures as a strong antibacterial agent and self-cleaning cover: synthesis, characterization and investigation of photocatalytic activity under UV irradiation. J Photochem Photobiol B Biol 178:512–520. https://doi.org/10.1016/j.jphotobiol.2017.12.008

Hosseini F, Assadi AA, Nguyen-Tri P et al (2022) Titanium-based photocatalytic coatings for bacterial disinfection: the shift from suspended powders to catalytic interfaces. Surf Interfaces 32:102078. https://doi.org/10.1016/j.surfin.2022.102078

Houas A, Lachheb H, Ksibi M et al (2001) Photocatalytic degradation pathway of methylene blue in water. Appl Catal B Environ 31:145–157. https://doi.org/10.1016/S0926-3373(00)00276-9

Hu Z, Yang C, Lv K et al (2020) Single atomic Au induced dramatic promotion of the photocatalytic activity of TiO_2 hollow microspheres. Chem Commun 56:1745–1748. https://doi.org/10.1039/c9cc08578e

Huang Z, Maness PC, Blake DM et al (2000) Bactericidal mode of titanium dioxide photocatalysis. J Photochem Photobiol A Chem 130:163–170. https://doi.org/10.1016/S1010-6030(99)00205-1

Hussein FH (2012) Comparison between solar and artificial photocatalytic decolorization of textile industrial wastewater. Int J Photoenergy 2012:Article ID 793648, 10 pages. https://doi.org/10.1155/2012/793648

Ibrahim RK, Hayyan M, AlSaadi MA et al (2016) Environmental application of nanotechnology: air, soil, and water. Environ Sci Pollut Res 23:13754–13788. https://doi.org/10.1007/s11356-016-6457-z

Jafri NNM, Jaafar J, Alias NH, et al (2021) Synthesis and characterization of titanium dioxide hollow nanofiber for photocatalytic degradation of methylene blue dye. Membranes (Basel) 11. https://doi.org/10.3390/membranes11080581

Jahanara K, Farhadi S (2019) A magnetically separable plate-like cadmium titanate-copper ferrite nanocomposite with enhanced visible-light photocatalytic degradation performance for organic contaminants. RSC Adv 9:15615–15628. https://doi.org/10.1039/c9ra01968e

Ji Y, Chen Z, Wei R, et al (2022) Selective CO-to-acetate electroreduction via intermediate adsorption tuning on ordered Cu–Pd sites. Nat Catal 2022 1–8. https://doi.org/10.1038/s41929-022-00757-8

Jing L, Xu Y, Huang S et al (2016) Novel magnetic $CoFe_2O_4$/Ag/Ag_3VO_4 composites: highly efficient visible light photocatalytic and antibacterial activity. Appl Catal B Environ 199:11–22. https://doi.org/10.1016/j.apcatb.2016.05.049

Karim AV, Hassani A, Eghbali P, Nidheesh PV (2022) Nanostructured modified layered double hydroxides (LDHs)-based catalysts: a review on synthesis, characterization, and applications in water remediation by advanced oxidation processes. Curr Opin Solid State Mater Sci 26:100965. https://doi.org/10.1016/j.cossms.2021.100965

Khairkar SR, Pansare AV, Shedge AA et al (2020) Hydrophobic interpenetrating polyamide-PDMS membranes for desalination, pesticides removal and enhanced chlorine tolerance. Chemosphere 258:127179. https://doi.org/10.1016/j.chemosphere.2020.127179

Khan MM, Adil SF, Al-Mayouf A (2015) Metal oxides as photocatalysts. J Saudi Chem Soc 19:462–464. https://doi.org/10.1016/j.jscs.2015.04.003

Khaw JS, Curioni M, Skeldon P, et al (2019) A novel methodology for economical scale-up of TiO_2 nanotubes fabricated on Ti and Ti alloys. J Nanotechnol 2019:38–40. https://doi.org/10.1155/2019/5902346

Kiayi Z, Lotfabad TB, Heidarinasab A, Shahcheraghi F (2019) Microbial degradation of azo dye carmoisine in aqueous medium using Saccharomyces cerevisiae ATCC 9763. J Hazard Mater 373:608–619. https://doi.org/10.1016/j.jhazmat.2019.03.111

Kim DS, Kwak SY (2007) The hydrothermal synthesis of mesoporous TiO_2 with high crystallinity, thermal stability, large surface area, and enhanced photocatalytic activity. Appl Catal A Gen 323:110–118. https://doi.org/10.1016/J.APCATA.2007.02.010

Kirankumar VS, Sumathi S (2020) A review on photodegradation of organic pollutants using spinel oxide. Mater Today Chem 18:100355. https://doi.org/10.1016/j.mtchem.2020.100355

Kiriakidou F, Kondarides D, Verykios XE et al (1999) The effect of operational parameters and TiO_2-doping on the photocatalytic degradation of azo-dyes. Catal Today 54:119–130 https://doi.org/10.1016/S0920-5861(99)00174-1

Kivrak H, Saleh DI, Alpaslan D, et al (2021) Quantum size effect of cadmium-doped titanium dioxide photocatalysts towards methylene blue degradation and electrooxidation. Int J Environ Sci Technol 1–12. https://doi.org/10.1007/S13762-021-03811-3/FIGURES/8

Kiwi J, Rtimi S (2021) Insight into the interaction of magnetic photocatalysts with the incoming light accelerating bacterial inactivation and environmental cleaning. Appl Catal B Environ 281:119420. https://doi.org/10.1016/j.apcatb.2020.119420

Konstantinou IK, Albanis TA (2004) TiO_2-assisted photocatalytic degradation of azo dyes in aqueous solution: kinetic and mechanistic investigations: a review. Appl Catal B Environ 49:1–14. https://doi.org/10.1016/J.APCATB.2003.11.010

Krishna Chandar N, Jayavel R (2014) Synthesis and characterization of C14TAB passivated cerium oxide nanoparticles prepared by co-precipitation route. Phys E Low-Dimens Syst Nanostruct 58:48–51. https://doi.org/10.1016/J.PHYSE.2013.10.040

Kuang D, Brillet J, Chen P et al (2008) Application of highly ordered TiO_2 nanotube arrays in flexible dye-sensitized solar cells. ACS Nano 2:1113–1116. https://doi.org/10.1021/nn800174y

Kudo T, Nakamura Y, Ruike A (2003) Development of rectangular column structured titanium oxide photocatalysts anchored on silica sheets by a wet process. Res Chem Intermed 296(29):631–639. https://doi.org/10.1163/156856703322539663

Kumar A (2017) A review on the factors affecting the photocatalytic degradation of hazardous materials. Mater Sci Eng Int J 1:106–114. https://doi.org/10.15406/mseij.2017.01.00018

Kumar M, Kumar V, Singh R (2017a) Diameter tuning of β -Ga_2O_3 nanowires using chemical vapor deposition technique. Nanoscale Res Lett 12:1–10. https://doi.org/10.1186/s11671-017-1915-1

Kumar V, Mohan S, Singh DK et al (2017b) Photo-mediated optimized synthesis of silver nanoparticles for the selective detection of Iron(III), antibacterial and antioxidant activity. Mater Sci Eng C 71:1004–1019. https://doi.org/10.1016/J.MSEC.2016.11.013

Lai Y, Meng M, Yu Y (2010) One-step synthesis, characterizations and mechanistic study of nanosheets-constructed fluffy ZnO and Ag/ZnO spheres used for rhodamine B photodegradation. Appl

Catal B Environ 100:491–501. https://doi.org/10.1016/j.apcatb.2010.08.027

Lawless D, Serpone N, Meisel D (1991) Role of $OH^{\cdot}$ radicals and trapped holes in photocatalysis. A pulse radiolysis study. J Phys Chem 95:5166–5170. https://doi.org/10.1021/J100166A047

Lee K, Lee NH, Shin SH et al (2006) Hydrothermal synthesis and photocatalytic characterizations of transition metals doped nano TiO_2 sols. Mater Sci Eng B Solid-State Mater Adv Technol 129:109–115. https://doi.org/10.1016/j.mseb.2005.12.032

Lei XF, Xue XX, Yang H et al (2015) Effect of calcination temperature on the structure and visible-light photocatalytic activities of (N, S and C) co-doped TiO_2 nano-materials. Appl Surf Sci 332:172–180. https://doi.org/10.1016/j.apsusc.2015.01.110

Lei XF, Xue XX, Yang H (2014) Preparation and characterization of Ag-doped TiO_2 nanomaterials and their photocatalytic reduction of Cr(VI) under visible light. Appl Surf Sci 321:396–403. https://doi.org/10.1016/j.apsusc.2014.10.045

Li C, Yuan J, Han B et al (2010) TiO_2 nanotubes incorporated with CdS for photocatalytic hydrogen production from splitting water under visible light irradiation. Int J Hydrogen Energy 35:7073–7079. https://doi.org/10.1016/j.ijhydene.2010.01.008

Li N, Tang S, Rao Y et al (2018a) Improved dye removal and simultaneous electricity production in a photocatalytic fuel cell coupling with persulfate activation. Electrochim Acta 270:330–338. https://doi.org/10.1016/j.electacta.2018.03.083

Li X, Liu G, Zhao J (1999) Two competitive primary processes in the photodegradation of cationic triarylmethane dyes under visible irradiation in TiO_2 dispersions. New J Chem 23:1193–1196. https://doi.org/10.1039/A906765E

Li X, Pustulka S, Pedu S, et al (2018b) Titanium dioxide nanotubes as model systems for electrosorption studies. Nanomaterials 8. https://doi.org/10.3390/nano8060404

Li X, Wu X, Liu S et al (2020a) Effects of fluorine on photocatalysis. Chinese J Catal 41:1451–1467. https://doi.org/10.1016/S1872-2067(20)63594-X

Li X, Yang H, Lv K, et al (2020b) Fabrication of porous TiO_2 nanosheets assembly for improved photoreactivity towards X3B dye degradation and NO oxidation. Appl Surf Sci 503:144080. https://doi.org/10.1016/j.apsusc.2019.144080

Lin C, Chen S, Cao L (2013) Anodic formation of aligned and bamboo-type TiO_2 nanotubes at constant low voltages. Mater Sci Semicond Process 16:154–159. https://doi.org/10.1016/j.mssp.2012.05.009

Lin H, Huang CP, Li W et al (2006) Size dependency of nanocrystalline TiO_2 on its optical property and photocatalytic reactivity exemplified by 2-chlorophenol. Appl Catal B Environ 68:1–11. https://doi.org/10.1016/J.APCATB.2006.07.018

Linder M, Theurich J, Bahnemann DW et al (1997) Photocatalytic degradation of organic compounds: accelerating the process efficiency. Water Sci Technol 35:79-86. https://doi.org/10.1016/S0273-1223(97)00012-7

Ling AL, Pace NR, Hernandez MT, Lapara TM (2013) Tetracycline resistance and class 1 integron genes associated with indoor and outdoor aerosols. Environ Sci Technol 47:4046–4052. https://doi.org/10.1021/es400238g

Liu L, Chen Z, Zhang J et al (2021) Treatment of industrial dye wastewater and pharmaceutical residue wastewater by advanced oxidation processes and its combination with nanocatalysts: a review. J Water Process Eng 42:102122. https://doi.org/10.1016/j.jwpe.2021.102122

Liu Y, Sun L, Wu J et al (2015) Preparation and photocatalytic activity of ZnO/Fe_2O_3 nanotube composites. Mater Sci Eng B Solid-State Mater Adv Technol 194:9–13. https://doi.org/10.1016/j.mseb.2014.12.021

Lozano A, Garcia J, Dormènech X, Casado J (1992) Heterogeneous photocatalytic oxidation of manganese(II) over TiO_2. J Photochem Photobiol A Chem 69:237–240. https://doi.org/10.1016/1010-6030(92)85283-Z

Lu HB, Li H, Liao L et al (2008) Low-temperature synthesis and photocatalytic properties of ZnO nanotubes by thermal oxidation of Zn nanowires. Nanotechnology 19:13–20. https://doi.org/10.1088/0957-4484/19/04/045605

Lu Y, Ou X, Wang W et al (2020) Fabrication of TiO_2 nanofiber assembly from nanosheets (TiO_2-NFs-NSs) by electrospinning-hydrothermal method for improved photoreactivity. Chinese J Catal 41:209–218. https://doi.org/10.1016/S1872-2067(19)63470-4

Luo H, Xu P, Roane TM et al (2012) Microbial desalination cells for improved performance in wastewater treatment, electricity production, and desalination. Bioresour Technol 105:60–66. https://doi.org/10.1016/j.biortech.2011.11.098

Luo S, Xiao Y, Yang L et al (2011) Simultaneous detoxification of hexavalent chromium and acid orange 7 by a novel Au/TiO_2 heterojunction composite nanotube arrays. Sep Purif Technol 79:85–91. https://doi.org/10.1016/j.seppur.2011.03.019

Madihi-Bidgoli S, Asadnezhad S, Yaghoot-Nezhad A, Hassani A (2021) Azurobine degradation using Fe_2O_3@multi-walled carbon nanotube activated peroxymonosulfate (PMS) under UVA-LED irradiation: performance, mechanism and environmental application. J Environ Chem Eng 9:106660. https://doi.org/10.1016/j.jece.2021.106660

Madona J, Sridevi C (2022) Surfactant assisted hydrothermal synthesis of MgO/g-C_3N_4 heterojunction nanocomposite for enhanced solar photocatalysis and antimicrobial activities. Inorg Chem Commun 138:109265. https://doi.org/10.1016/j.inoche.2022.109265

Maity S, Banerjee D, Bhattacharya G et al (2022) Hydrothermally synthesized sulfur-doped graphite as supercapacitor electrode materials. ACS Appl Nano Mater. https://doi.org/10.1021/ACSANM.1C04169/SUPPL_FILE/AN1C04169_SI_002.PDF

Malik SN, Ghosh PC, Vaidya AN, Mudliar SN (2020) Hybrid ozonation process for industrial wastewater treatment: principles and applications: a review. J Water Process Eng 35. https://doi.org/10.1016/j.jwpe.2020.101193

Mamba G, Mishra A (2016) Advances in magnetically separable photocatalysts: smart, recyclable materials for water pollution mitigation. Catalysts 6:1–34. https://doi.org/10.3390/catal6060079

Mandal RK, Purkayastha MD, Pal Majumder T (2019) Silver modified cadmium oxide – a novel material for enhanced photodegradation of malachite green. Optik (stuttg) 180:174–182. https://doi.org/10.1016/J.IJLEO.2018.11.066

Mandor H, Amin NK, Abdelwahab O et al (2022) Preparation and characterization of N-doped ZnO and N-doped TiO_2 beads for photocatalytic degradation of phenol and ammonia. Environ Sci Pollut Res 1:1–18. https://doi.org/10.1007/S11356-022-19421-6

Mani SK, Manickam S, Muthusamy V, Thangaraj R (2018) Antimicrobial activity and photocatalytic degradation properties of zinc sulfide nanoparticles synthesized by using plant extracts. J Nanostructures 8:107–118. https://doi.org/10.22052/JNS.2018.02.001

Meng F, Song X, Sun Z (2009) Photocatalytic activity of TiO_2 thin films deposited by RF magnetron sputtering. Vacuum 83:1147–1151. https://doi.org/10.1016/j.vacuum.2009.02.009

Miklos DB, Remy C, Jekel M et al (2018) Evaluation of advanced oxidation processes for water and wastewater treatment – a critical review. Water Res 139:118–131. https://doi.org/10.1016/j.watres.2018.03.042

Mills A (2012) An overview of the methylene blue ISO test for assessing the activities of photocatalytic films. Appl Catal B Environ 128:144–149. https://doi.org/10.1016/j.apcatb.2012.01.019

Mills A, Belghazi A, Rodman D (1996) Bromate removal from drinking water by semiconductor photocatalysis. Water Res 30:1973–1978. https://doi.org/10.1016/0043-1354(96)00012-7

Mojiri A, Zhou JL, Ohashi A et al (2019) Comprehensive review of polycyclic aromatic hydrocarbons in water sources, their effects and treatments. Sci Total Environ 696:133971. https://doi.org/10.1016/j.scitotenv.2019.133971

Mondal P, Bhowmick S, Chatterjee D et al (2013) Remediation of inorganic arsenic in groundwater for safe water supply: a critical assessment of technological solutions. Chemosphere 92:157–170. https://doi.org/10.1016/j.chemosphere.2013.01.097

Munyai S, Hintsho-Mbita NC (2021) Green derived metal sulphides as photocatalysts for waste water treatment. A review. Curr Res Green Sustain Chem 4:100163. https://doi.org/10.1016/j.crgsc.2021.100163

Murugan R, Kashinath L, Subash R et al (2018) Pure and alkaline metal ion (Mg, Ca, Sr, Ba) doped cerium oxide nanostructures for photo degradation of methylene blue. Mater Res Bull 97:319–325. https://doi.org/10.1016/J.MATERRESBULL.2017.09.026

Nabi SA, Shahadat M, Bushra R et al (2010) Development of composite ion-exchange adsorbent for pollutants removal from environmental wastes. Chem Eng J 165:405–412. https://doi.org/10.1016/j.cej.2010.08.068

Nakkala JR, Bhagat E, Suchiang K, Sadras SR (2015) Comparative study of antioxidant and catalytic activity of silver and gold nanoparticles synthesized from Costus pictus leaf extract. J Mater Sci Technol 31:986–994. https://doi.org/10.1016/J.JMST.2015.07.002

Nataraj SK, Hosamani KM, Aminabhavi TM (2006) Distillery wastewater treatment by the membrane-based nanofiltration and reverse osmosis processes. Water Res 40:2349–2356. https://doi.org/10.1016/j.watres.2006.04.022

Natarajan S, Bajaj HC, Tayade RJ (2018) Recent advances based on the synergetic effect of adsorption for removal of dyes from waste water using photocatalytic process. J Environ Sci (china) 65:201–222. https://doi.org/10.1016/j.jes.2017.03.011

Neena D, Kondamareddy KK, Bin H et al (2018) Enhanced visible light photodegradation activity of RhB/MB from aqueous solution using nanosized novel Fe-Cd co-modified ZnO. Sci Rep 8:1–12. https://doi.org/10.1038/s41598-018-29025-1

Nesic J, Rtimi S, Laub D et al (2014) New evidence for TiO_2 uniform surfaces leading to complete bacterial reduction in the dark: critical issues. Colloids Surfaces B Biointerfaces 123:593–599. https://doi.org/10.1016/j.colsurfb.2014.09.060

Nidheesh PV, Gandhimathi R, Ramesh ST (2013) Degradation of dyes from aqueous solution by Fenton processes: a review. Environ Sci Pollut Res 20:2099–2132. https://doi.org/10.1007/s11356-012-1385-z

Nidheesh PV, Scaria J, Babu DS, Kumar MS (2021) An overview on combined electrocoagulation-degradation processes for the effective treatment of water and wastewater. Chemosphere 263:127907. https://doi.org/10.1016/j.chemosphere.2020.127907

Nogier JP, Delamar M (1994) Chapter 7.1 X-ray photoelectron spectroscopy of TiO_2/V_2O_5 catalysts. Catal Today 20:109–123. https://doi.org/10.1016/0920-5861(94)85020-8

Noorisepehr M, Kakavandi B, Isari AA et al (2020) Sulfate radical-based oxidative degradation of acetaminophen over an efficient hybrid system: peroxydisulfate decomposed by ferroferric oxide nanocatalyst anchored on activated carbon and UV light. Sep Purif Technol 250:116950. https://doi.org/10.1016/j.seppur.2020.116950

Ottman N, Ruokolainen L, Suomalainen A et al (2019) Soil exposure modifies the gut microbiota and supports immune tolerance in a mouse model. J Allergy Clin Immunol 143:1198-1206.e12. https://doi.org/10.1016/J.JACI.2018.06.024

Oturan MA, Aaron JJ (2014) Advanced oxidation processes in water/wastewater treatment: principles and applications. A review. Crit Rev Environ Sci Technol 44:2577–2641. https://doi.org/10.1080/10643389.2013.829765

Paola AD, Bellardita M, Palmisano L (2013) Brookite, the least known TiO_2 photocatalyst. Catalysts LP 3:36–73. https://doi.org/10.3390/catal3010036

Parnicka P, Mazierski P, Lisowski W et al (2019) A new simple approach to prepare rare-earth metals-modified TiO_2 nanotube arrays photoactive under visible light: surface properties and mechanism investigation. Results Phys 12:412–423. https://doi.org/10.1016/j.rinp.2018.11.073

Parsons JG, Lopez ML, Peralta-Videa JR, Gardea-Torresdey JL (2009) Determination of arsenic(III) and arsenic(V) binding to microwave assisted hydrothermal synthetically prepared Fe_3O_4, Mn_3O_4, and $MnFe_2O_4$ nanoadsorbents. Microchem J 91:100–106. https://doi.org/10.1016/j.microc.2008.08.012

Patete JM, Peng X, Koenigsmann C et al (2011) Viable methodologies for the synthesis of high-quality nanostructures. Green Chem 13:482–519. https://doi.org/10.1039/C0GC00516A

Pera-Titus M, García-Molina V, Baños MA et al (2004) Degradation of chlorophenols by means of advanced oxidation processes: a general review. Appl Catal B Environ 47:219–256. https://doi.org/10.1016/J.APCATB.2003.09.010

Perry SC, Pangotra D, Vieira L et al (2019) Electrochemical synthesis of hydrogen peroxide from water and oxygen. Nat Rev Chem 37(3):442–458. https://doi.org/10.1038/s41570-019-0110-6

Pham Xuan N, Nguyen Thi H, Nguyen Trung T et al (2020) Synthesis of Ag-TiO_2/perlite composite for the photodegradation of methylene blue under solar light irradiation. Vietnam J Catal Adsorpt 9:42–48. https://doi.org/10.51316/JCA.2020.068

Pillai SC, Periyat P, George R et al (2007) Synthesis of high-temperature stable anatase TiO_2 photocatalyst. J Phys Chem C 111:1605–1611. https://doi.org/10.1021/jp065933h

Pirkarami A, Olya ME, Raeis Farshid S (2014) UV/Ni-TiO_2 nanocatalyst for electrochemical removal of dyes considering operating costs. Water Resour Ind 5:9–20. https://doi.org/10.1016/j.wri.2014.02.001

Pourshirband N, Nezamzadeh-Ejhieh A (2021) An efficient Z-scheme CdS/g-C_3N_4 nano catalyst in methyl orange photodegradation: focus on the scavenging agent and mechanism. J Mol Liq 335:116543. https://doi.org/10.1016/j.molliq.2021.116543

Rajendrachari S, Taslimi P, Karaoglanli AC et al (2021) Photocatalytic degradation of rhodamine B (RhB) dye in waste water and enzymatic inhibition study using cauliflower shaped ZnO nanoparticles synthesized by a novel one-pot green synthesis method. Arab J Chem 14:103180. https://doi.org/10.1016/J.ARABJC.2021.103180

Ramya A, Dhevagi P, Rakesh SS (2022) Nanomaterials for wastewater remediation: resolving huge problems with tiny particles. Nanotechnol 601–620. https://doi.org/10.1007/978-3-030-80371-1_21

Rana S, Gupta N, Rana RS (2018) Removal of organic pollutant with the use of rotating biological contactor. Mater Today Proc 5:4218–4224. https://doi.org/10.1016/j.matpr.2017.11.685

Rao NH, Lakshmidevi N, Pammi SVN et al (2016) Green synthesis of silver nanoparticles using methanolic root extracts of Diospyros paniculata and their antimicrobial activities. Mater Sci Eng C 62:553–557. https://doi.org/10.1016/J.MSEC.2016.01.072

Rasheed T, Bilal M, Iqbal HMN, et al (2017) Reaction mechanism and degradation pathway of rhodamine 6G by photocatalytic treatment. Water Air Soil Pollut 228. https://doi.org/10.1007/s11270-017-3458-6

Real FJ, Acero JL, Benitez FJ et al (2010) Oxidation of hydrochlorothiazide by UV radiation, hydroxyl radicals and ozone: kinetics and elimination from water systems. Chem Eng J 160:72–78. https://doi.org/10.1016/j.cej.2010.03.009

Reardon S (2014) Antibiotic resistance sweeping developing world. Nature 509:141–142. https://doi.org/10.1038/509141a

Reemtsma T, Weiss S, Mueller J et al (2006) Polar pollutants entry into the water cycle by municipal wastewater: a European perspective.

Environ Sci Technol 40:5451–5458. https://doi.org/10.1021/es060908a

Regkouzas P, Diamadopoulos E (2019) Adsorption of selected organic micro-pollutants on sewage sludge biochar. Chemosphere 224:840–851. https://doi.org/10.1016/j.chemosphere.2019.02.165

Rioja N, Zorita S, Peñas FJ (2016) Effect of water matrix on photocatalytic degradation and general kinetic modeling. Appl Catal B Environ 180:330–335. https://doi.org/10.1016/j.apcatb.2015.06.038

Robinson Aguirre O, Félix Echeverría E (2018) Effects of fluoride source on the characteristics of titanium dioxide nanotubes. Appl Surf Sci 445:308–319. https://doi.org/10.1016/j.apsusc.2018.03.139

Rojviroon T, Rojviroon O, Sirivithayapakorn S (2015) Photocatalytic decolourisation of dyes using TiO_2 thin film photocatalysts. Surf Eng 32:562–569. https://doi.org/10.1179/1743294415Y.0000000096

Rojviroon T, Rojviroon O, Sirivithayapakorn S (2021) Application of TiO_2 nanotubes as photocatalysts for decolorization of synthetic dye wastewater. Water Resour Ind 26:100163. https://doi.org/10.1016/j.wri.2021.100163

Rtimi S, Giannakis S, Bensimon M et al (2016) Supported TiO_2 films deposited at different energies: implications of the surface compactness on the catalytic kinetics. Appl Catal B Environ 191:42–52. https://doi.org/10.1016/j.apcatb.2016.03.019

Rtimi S, Pulgarin C, Sanjines R, Kiwi J (2015) Applied catalysis B : environmental kinetics and mechanism for transparent polyethylene-TiO_2 films mediated self-cleaning leading to MB dye discoloration under sunlight irradiation. "Applied Catal B. Environ 162:236–244. https://doi.org/10.1016/j.apcatb.2014.05.039

Sabhi S, Kiwi J (2001) Degradation of 2,4-dichlorophenol by immobilized iron catalysts. Water Res 35:1994–2002. https://doi.org/10.1016/S0043-1354(00)00460-7

Saikia L, Bhuyan D, Saikia M et al (2015) Photocatalytic performance of ZnO nanomaterials for self sensitized degradation of malachite green dye under solar light. Appl Catal A Gen 490:42–49. https://doi.org/10.1016/J.APCATA.2014.10.053

Sakimoto KK, Wong AB, Yang P et al (2016) Self-photosensitization of nonphotosynthetic bacteria for solar-to-chemical production. Science 351:74–77. https://doi.org/10.1126/science.aad3317

Saleh R, Djaja NF (2014) UV light photocatalytic degradation of organic dyes with Fe-doped ZnO nanoparticles. Superlattices Microstruct 74:217–233. https://doi.org/10.1016/J.SPMI.2014.06.013

Sanna V, Pala N, Alzari V et al (2016) ZnO nanoparticles with high degradation efficiency of organic dyes under sunlight irradiation. Mater Lett 162:257–260. https://doi.org/10.1016/J.MATLET.2015.10.031

Selvasembian R, Balasubramanian P (2018) Utilization of unconventional lignocellulosic waste biomass for the biosorption of toxic triphenylmethane dye malachite green from aqueous solution 20:624–633. https://doi.org/10.1080/15226514.2017.1413329

Shabaan OA, Jahin HS, Mohamed GG (2020) Removal of anionic and cationic dyes from wastewater by adsorption using multiwall carbon nanotubes. Arab J Chem 13:4797–4810. https://doi.org/10.1016/J.ARABJC.2020.01.010

Shah P, Joshi K, Shah M et al (2022) Photocatalytic dye degradation using nickel ferrite spinel and its nanocomposite. Environ Sci Pollut Res. https://doi.org/10.1007/s11356-022-21248-0

Shammi ZM, Kianfar A, Momeni MM (2021) Photocatalytic degradation and mineralization of dye pollutants from wastewater under visible light using synthetic CuO-VO_2/TiO_2 nanotubes/nanosheets. J Mater Sci Mater Electron 32:20149–20163. https://doi.org/10.1007/S10854-021-06486-1/SCHEMES/2

Sharma P, Hussain N, Borah DJ, Das MR (2013) Kinetics and adsorption behavior of the methyl blue at the graphene oxide/reduced graphene oxide nanosheet-water interface: a comparative study. J Chem Eng Data 58:3477–3488. https://doi.org/10.1021/je400743r

Sharma R (2021) Synthesis of Terminalia bellirica fruit extract mediated silver nanoparticles and application in photocatalytic degradation of wastewater from textile industries. Mater Today Proc 44:1995–1998. https://doi.org/10.1016/J.MATPR.2020.12.118

Shirley DA (1972) High-resolution x-ray photoemission spectrum of the valence bands of gold. Phys Rev B 5:4709–4714. https://doi.org/10.1103/PhysRevB.5.4709

Siddique M, Khan R, Khan AF, Farooq R (2014) Improved photocatalytic activity of TiO_2 coupling ultrasound for Reactive Blue 19 degradation. J Chem Soc Pakistan 36:37–43

Singh P, Shandilya P, Raizada P et al (2020) Review on various strategies for enhancing photocatalytic activity of graphene based nanocomposites for water purification. Arab J Chem 13:3498–3520. https://doi.org/10.1016/J.ARABJC.2018.12.001

Sirajudheen P, Karthikeyan P, Ramkumar K, Meenakshi S (2020) Effective removal of organic pollutants by adsorption onto chitosan supported graphene oxide-hydroxyapatite composite: a novel reusable adsorbent. J Mol Liq 318:114200. https://doi.org/10.1016/j.molliq.2020.114200

Sobczyński A, Dobosz A (2001) Water purification by photocatalysis on semiconductors. Polish J Environ Stud 10:195–205

Sopha H, Krbal M, Ng S et al (2017) Highly efficient photoelectrochemical and photocatalytic anodic TiO_2 nanotube layers with additional TiO_2 coating. Appl Mater Today 9:104–110. https://doi.org/10.1016/j.apmt.2017.06.002

Sorensen L, Strouse GF, Stiegman AE (2006) Fabrication of stable low-density silica aerogels containing luminescent ZnS capped CdSe quantum dots. Adv Mater 18:1965–1967. https://doi.org/10.1002/ADMA.200600791

Suhaimy SHM, Lai CW, Tajuddin HA et al (2018) Impact of TiO_2 nanotubes' morphology on the photocatalytic degradation of simazine pollutant. Materials (basel) 11:1–15. https://doi.org/10.3390/ma11112066

Suksabye P, Thiravetyan P, Nakbanpote W, Chayabutra S (2007) Chromium removal from electroplating wastewater by coir pith. J Hazard Mater 141:637–644. https://doi.org/10.1016/j.jhazmat.2006.07.018

Sun J, Qiao L, Sun S, Wang G (2008) Photocatalytic degradation of Orange G on nitrogen-doped TiO_2 catalysts under visible light and sunlight irradiation. J Hazard Mater 155:312–319. https://doi.org/10.1016/J.JHAZMAT.2007.11.062

Sun M, Han X, Chen S (2019) Synthesis and photocatalytic activity of nano-cobalt ferrite catalyst for the photo-degradation various dyes under simulated sunlight irradiation. Mater Sci Semicond Process 91:367–376. https://doi.org/10.1016/j.mssp.2018.12.005

Sun Q, Li H, Zheng S, Sun Z (2014) Characterizations of nano-TiO_2/diatomite composites and their photocatalytic reduction of aqueous Cr (VI). Appl Surf Sci 311:369–376. https://doi.org/10.1016/j.apsusc.2014.05.070

Surenjan A, Pradeep T, Philip L (2019) Application and performance evaluation of a cost-effective vis- LED based fluidized bed reactor for the treatment of emerging contaminants. Chemosphere 228:629–639. https://doi.org/10.1016/j.chemosphere.2019.04.179

Tang F, Yu H, Yassin Hussain Abdalkarim S et al (2020) Green acid-free hydrolysis of wasted pomelo peel to produce carboxylated cellulose nanofibers with super absorption/flocculation ability for environmental remediation materials. Chem Eng J 395:125070. https://doi.org/10.1016/j.cej.2020.125070

Tatarchuk T, Mironyuk I, Kotsyubynsky V et al (2020) Structure, morphology and adsorption properties of titania shell immobilized

onto cobalt ferrite nanoparticle core. J Mol Liq 297:111757. https://doi.org/10.1016/j.molliq.2019.111757
Teh CY, Budiman PM, Shak KPY, Wu TY (2016) Recent advancement of coagulation-flocculation and its application in wastewater treatment. Ind Eng Chem Res 55:4363–4389. https://doi.org/10.1021/acs.iecr.5b04703
Thilagavathi T, Venugopal D, Marnadu R, Chandrasekaran J, Thangaraju D, Palanivel B, Hamdy MS, M. Shkir M, Ali HE, et al (2021) $WO_3/CoWO_4$ nanocomposite synthesis using a facile co-precipitation method for enhanced photocatalytic applications. J Phys Chem Solids 154:110066. https://doi.org/10.1016/j.jpcs.2021.110066
Thiruvenkatachari R, Vigneswaran S, Moon IS (2008) A review on UV/TiO_2 photocatalytic oxidation process (Journal Review). Korean J Chem Eng 25:64–72. https://doi.org/10.1007/S11814-008-0011-8
Trellu C, Olvera Vargas H, Mousset E et al (2021) Electrochemical technologies for the treatment of pesticides. Curr Opin Electrochem 26:100677. https://doi.org/10.1016/j.coelec.2020.100677
Ullah A, Rasheed S, Ali I, Ullah N (2021) Plant mediated synthesis of CdS nanoparticles, their characterization and application for photocatalytic degradation of toxic organic dye. Chem Rev Lett 4:98–107. https://doi.org/10.22034/CRL.2021.262754.1097
Van Dao D, Nguyen TTD, Majhi SM et al (2019) Ionic liquid-supported synthesis of CeO_2 nanoparticles and its enhanced ethanol gas sensing properties. Mater Chem Phys 231:1–8. https://doi.org/10.1016/J.MATCHEMPHYS.2019.03.025
Van VP, Phan BT, Mott D et al (2018) Silver nanoparticle loaded TiO_2 nanotubes with high photocatalytic and antibacterial activity synthesized by photoreduction method. J Photochem Photobiol A Chem 352:106–112. https://doi.org/10.1016/j.jphotochem.2017.10.051
Wang D, Astruc D (2017) The recent development of efficient Earth-abundant transition-metal nanocatalysts. Chem Soc Rev 46:816–854. https://doi.org/10.1039/c6cs00629a
Wang F, Liu J, Wang X et al (2012a) Alpha-Fe_2O_3@ZnO heterostructured nanotubes for gas sensing. Mater Lett 76:159–161. https://doi.org/10.1016/j.matlet.2012.02.086
Wang H, Li G, Jia L et al (2008) Controllable preferential-etching synthesis and photocatalytic activity of porous ZnO nanotubes. J Phys Chem C 112:11738–11743. https://doi.org/10.1021/jp803059k
Wang J, Yang H, Jiang L et al (2018) Highly efficient removal of organic pollutants by ultrahigh-surface-area-ethynylbenzene-based conjugated microporous polymers via adsorption–photocatalysis synergy. Catal Sci Technol 8:5024–5033. https://doi.org/10.1039/C8CY01379A
Wang JL, Xu LJ (2012) Advanced oxidation processes for wastewater treatment: Formation of hydroxyl radical and application. Crit Rev Environ Sci Technol 42:251–325. https://doi.org/10.1080/10643389.2010.507698
Wang R, Wang X, Xi X, et al (2012b) Preparation and photocatalytic activity of magnetic $Fe_3O_4/SiO_2/TiO_2$ composites. Adv Mater Sci Eng 2012b. https://doi.org/10.1155/2012/409379
Wang X, Yu S, Li ZH et al (2021) Fabrication Z-scheme heterojunction of $Ag_2O/ZnWO_4$ with enhanced sonocatalytic performances for meloxicam decomposition: increasing adsorption and generation of reactive species. Chem Eng J 405:126922. https://doi.org/10.1016/j.cej.2020.126922
Wang YS, Shen JH, Horng JJ (2014) Chromate enhanced visible light driven TiO_2 photocatalytic mechanism on Acid Orange 7 photodegradation. J Hazard Mater 274:420–427. https://doi.org/10.1016/j.jhazmat.2014.04.042
Xiaosheng Fang B, Bando Y, Liao M et al (2009) Single-crystalline ZnS nanobelts as ultraviolet-light sensors. Wiley Online Libr 21:2034–2039. https://doi.org/10.1002/adma.200802441
Yadav S, Shakya K, Gupta A et al (2022) A review on degradation of organic dyes by using metal oxide semiconductors. Environ Sci Pollut Res. https://doi.org/10.1007/s11356-022-20818-6
Ye M, Zhang Q, Hu Y et al (2010a) Magnetically recoverable core-shell nanocomposites with enhanced photocatalytic activity. Chem - A Eur J 16:6243–6250. https://doi.org/10.1002/CHEM.200903516
Ye Y, Bruning H, Li X et al (2018) Significant enhancement of micropollutant photocatalytic degradation using a TiO_2 nanotube array photoanode based photocatalytic fuel cell. Chem Eng J 354:553–562. https://doi.org/10.1016/j.cej.2018.08.064
Yu J, Kiwi J, Wang T, et al (2019a) Duality in the mechanism of hexagonal zno/cuxo nanowires inducing sulfamethazine degradation under solar or visible light. Catalysts 9. https://doi.org/10.3390/catal9110916
Yu J, Kiwi J, Zivkovic I et al (2019b) Quantification of the local magnetized nanotube domains accelerating the photocatalytic removal of the emerging pollutant tetracycline. Appl Catal B Environ 248:450–458. https://doi.org/10.1016/j.apcatb.2019.02.046
Yu J, Sun D, Wang T, Li F (2018) Fabrication of Ag@AgCl/ZnO submicron wire film catalyst on glass substrate with excellent visible light photocatalytic activity and reusability. Chem Eng J 334:225–236. https://doi.org/10.1016/j.cej.2017.10.003
Yu J, Wang T, Rtimi S (2019c) Magnetically separable TiO_2/FeO_x/POM accelerating the photocatalytic removal of the emerging endocrine disruptor: 2,4-dichlorophenol. Appl Catal B Environ 254:66–75. https://doi.org/10.1016/j.apcatb.2019.04.088
Yu Q, Fu W, Yu C et al (2007) Fabrication and optical properties of large-scale ZnO nanotube bundles via a simple solution route. J Phys Chem C 111:17521–17526. https://doi.org/10.1021/jp076159g
Yunus NN, Hamzah F, So'Aib MS, Krishnan J (2017) Effect of catalyst loading on photocatalytic degradation of phenol by using N, S Co-doped TiO_2. IOP Conf Ser Mater Sci Eng 206. https://doi.org/10.1088/1757-899X/206/1/012092
Zanjanchi MA, Ebrahimian A, Arvand M (2010) Sulphonated cobalt phthalocyanine-MCM-41: an active photocatalyst for degradation of 2,4-dichlorophenol. J Hazard Mater 175:992–1000. https://doi.org/10.1016/j.jhazmat.2009.10.108
Zeghioud H, Assadi AA, Khellaf N, et al (2019) Photocatalytic performance of Cu_xO/TiO_2 deposited by HiPIMS on polyester under visible light LEDs: oxidants, ions effect, and reactive oxygen species investigation. Materials (Basel) 12. https://doi.org/10.3390/ma12030412
Zeghioud H, Khellaf N, Amrane A et al (2017) Photocatalytic performance of TiO_2 impregnated polyester for the degradation of Reactive Green 12: implications of the surface pretreatment and the microstructure. J Photochem Photobiol A Chem 346:493–501. https://doi.org/10.1016/j.jphotochem.2017.07.005
Zhang G, Zhang YC, Nadagouda M et al (2014) Visible light-sensitized S, N and C co-doped polymorphic TiO_2 for photocatalytic destruction of microcystin-LR. Appl Catal B Environ 144:614–621. https://doi.org/10.1016/j.apcatb.2013.07.058
Zhang J, Liu X, Wang L, et al (2011) Synthesis and gas sensing properties of α-Fe_2O_3@ZnO core-shell nanospindles. Nanotechnology 22. https://doi.org/10.1088/0957-4484/22/18/185501
Zhang S, Niu H, Cai Y et al (2010) Arsenite and arsenate adsorption on coprecipitated bimetal oxide magnetic nanomaterials:

$MnFe_2O_4$ and $CoFe_2O_4$. Chem Eng J 158:599–607. https://doi.org/10.1016/j.cej.2010.02.013

Zhang T, Liu Y, Zhong S, Zhang L (2020) AOPs-based remediation of petroleum hydrocarbons-contaminated soils: efficiency, influencing factors and environmental impacts. Chemosphere 246:125726. https://doi.org/10.1016/j.chemosphere.2019.125726

Zhang Y, Chu W (2022) Bisphenol S degradation via persulfate activation under UV-LED using mixed catalysts: synergistic effect of Cu–TiO_2 and Zn–TiO_2 for catalysis. Chemosphere 286:131797. https://doi.org/10.1016/j.chemosphere.2021.131797

Zhang YC, Yang M, Zhang G, Dionysiou DD (2013) HNO_3-involved one-step low temperature solvothermal synthesis of N-doped TiO_2 nanocrystals for efficient photocatalytic reduction of Cr(VI) in water. Appl Catal B Environ 142–143:249–258. https://doi.org/10.1016/j.apcatb.2013.05.023

Zhao S, Cheng Z, Kang L et al (2017) The facile preparation of Ag decorated TiO_2/ZnO nanotubes and their potent photocatalytic degradation efficiency. RSC Adv 7:50064–50071. https://doi.org/10.1039/c7ra09466c

Zhu G, Zhang S, Xu Z et al (2011) Ultrathin ZnS single crystal nanowires: controlled synthesis and room-temperature ferromagnetism properties. J Am Chem Soc 133:15605–15612. https://doi.org/10.1021/ja2049258

Zhu X, Castleberry SR, Nanny MA, Butler EC (2005) Effects of pH and catalyst concentration on photocatalytic oxidation of aqueous ammonia and nitrite in titanium dioxide suspensions. ACS Publ 39:3784–3791. https://doi.org/10.1021/es0485715

Zhu X, Yu X, Gao W et al (2022) Optical enhancement of nonstoichiometry-induced heterojunction in lanthanide doped double perovskite phosphors for WLEDs and scintillation applications. Chem Eng J 442:136235. https://doi.org/10.1016/J.CEJ.2022.136235